

## Research papers

# Optimal configuration of solar and wind-based hybrid renewable energy system with and without energy storage including environmental and social criteria: A case study

Shebaz A. Memon, Darshit S. Upadhyay, Rajesh N. Patel \*

Institute of Technology, Nirma University, Ahmedabad, Gujarat, India



## ARTICLE INFO

**Keywords:**

Hybrid renewable energy systems  
 Battery systems  
 Optimization  
 Carbon emission  
 Job creation  
 GRG method

## ABSTRACT

The Hybrid renewable energy system (HRES) has the potential to better match the demand load profile with power by using the complementary nature of the variable renewables. The sizing of the HRES should be done carefully to better match with demand load without oversizing and under-sizing. This study presents the use of the Generalized Reduced Gradient Method to optimize the size of components of HRES. The case study is performed to demonstrate the HRES for a remote rural region. Cases of both the standalone and grid-connected modes are explored. The standalone system with reliability from 100% up to 70% is investigated. A grid-connected system is studied with and without payment of power supplied to the grid to explore the feasibility of HRES for different price regimes. The methodology used is validated using HOMER software by comparing its results with HOMER results for the cases considered. Higher renewable share in the standalone systems leads to more need for employments at every stage of the lifecycle of components. In addition to that, the negative environmental impact of the HRES system in comparison to the conventional system is significantly less. It can be concluded that the standalone system proves to be better in terms of job creation and carbon emission. In contrast, grid-connected comes out to be better in terms of reliability and economics.

## 1. Introduction

The search for viable alternates to conventional energy extraction methods has become imperative. The technological advances in the manufacturing of solar photovoltaic panels and a large amount of production quantity have been decreasing their capital cost steadily for many years [1]. The issue of the intermittent supply of solar and wind energy, because of their dependence on the non-steady natural phenomenon has been the cause of concern. This issue has gained increased significance in the wake of the Paris agreement in 2015 [2], where member countries, including India, have agreed to substantially increase the share of renewables in their energy mix [3].

Putting together more than one energy resource with some energy storage facility can be the way forward to synchronize the demand and supply curves [4]. The combination of two or more renewable sources with or without conventional source and storage is called a hybrid renewable energy system (HRES), as shown in Fig. 1, where the complementarity of resources is harnessed to decrease the mismatch between the supply of individual energy sources and demand load [5].

The optimization technique should be able to handle the mathematical model of power production and other parameters of the HRES system. If the power production is not linearly correlated with renewable resource availability e.g., wind speed [6], then our optimization technique can't be linear programming. The optimization method ought to be capable of computing equations of cost and power production of HRES, as shown in the flow diagram of the general optimization process of HRES in Fig. 2.

The optimization techniques used for HRES are many [7] and can be categorized into conventional, modern, and hybrid techniques [8]. Classical optimization techniques try to find the global optimum of the set of the equations using mathematical formulations like nonlinear programming (NLP), Iterative techniques, etc. The advantage of these methods is that they provide definite answers, but the demerit is that they cannot handle a large number of variables. Criteria like negative environmental impact and social parameters like job creation are gaining the attention of researchers in addition to economic and reliability criteria. This adds complexity and subjectivity to the modeling of HRES. Artificial techniques like genetic algorithm (GA), Particle Swarm Optimization (PSO), and other evolutionary algorithms are needed to handle multi-criteria decision-making effectively. Many researchers have tried

\* Corresponding author.

E-mail address: [rajeshnpatel1969@yahoo.com](mailto:rajeshnpatel1969@yahoo.com) (R.N. Patel).

Nomenclature		c	Cell
HRES	Hybrid Renewable Energy System	<i>Symbols</i>	
VRE	Variable Renewable Energy	C	Capacity or size of the component
GRG	Generalized Reduced Gradient	Cu	Unit cost of the component
PV	Photovoltaic Panels	₹	Indian National Rupee
WT	Wind Turbine	\$	United States Dollar
BS	Battery System	i	Internal rate of return
COE	Cost of energy	E	Total energy in a year
CRF	Capital Recovery Factor	n	Life of the component
ALCC	Annual Life Cycle Cost	P	Power
RoE	Rate of Energy	η	Efficiency
NOCT	Nominal Operating Cell Temperature	I	Global Horizontal Irradiance
SA	Standalone system	T	Temperature
GC	Grid-connected system	V	Wind Speed
SOC	State of charge of battery	h	Hub Height
AEC	Annualized embodied carbon	A	Area
JC	Job creation	N	Number
<i>Subscript</i>		α	Surface roughness coefficient
j	Component of the system	cr	Cell reference
fg	From grid	ci	Cut-in
tg	To grid	co	Cut-out
L	Demand load	ch	Charging
r	Rated at the reference temperature	dch	Discharging

to combine two different optimization techniques to use the advantages of both, called hybrid techniques, which is an emerging field in the literature. The combination of solar energy and wind energy with or without other energy sources and storage techniques has been the dominant theme in the literature of HRES optimization. In recent years, attention has also been put on the demand side load management [9]. A variety of optimization methods are applied to the sizing optimization of HRES including newly developed ones like particle swarm optimization [10], cuckoo search [11], the crow algorithm [12], and gray wolf

optimization [13]. These methods are applied for a range of applications like electric vehicle charging [14], rural electrification [15], building applications [16], desalination [17], agricultural system [18], residential networks [19]. The modeling of the components should also be done keeping in mind the need of the HRES. The battery systems should be modeled and managed keeping in mind the empirical data provided by Deng et al. [20,21]. The energy management of the hybrid system was analyzed by Tang et al. [22,23].

The acquisition of power from renewable energy sources is not free

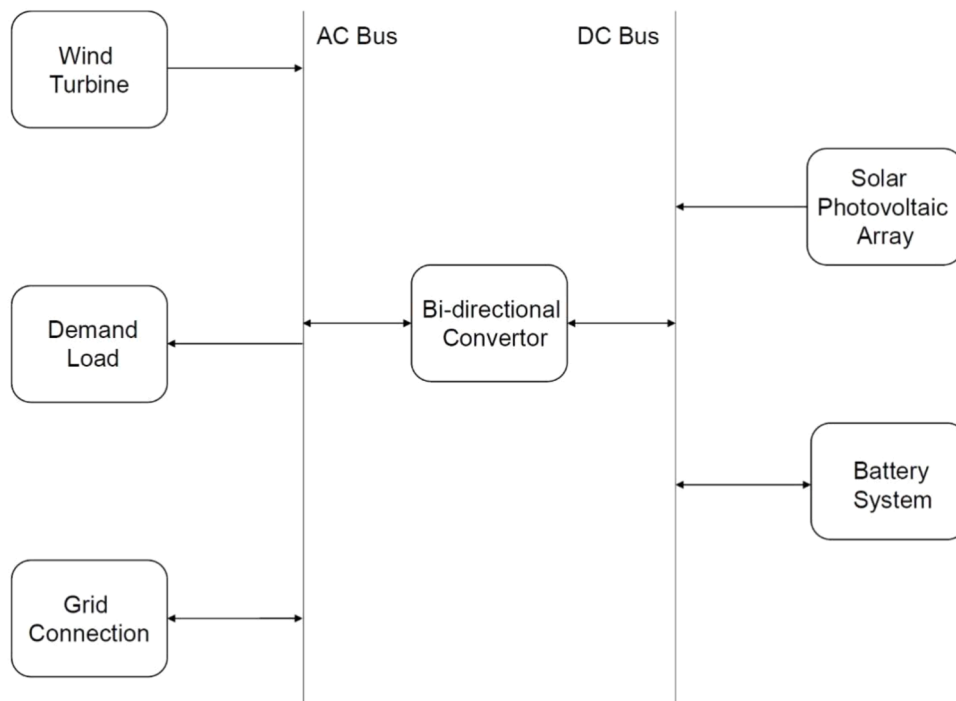


Fig. 1. Line diagram of typical HRES.

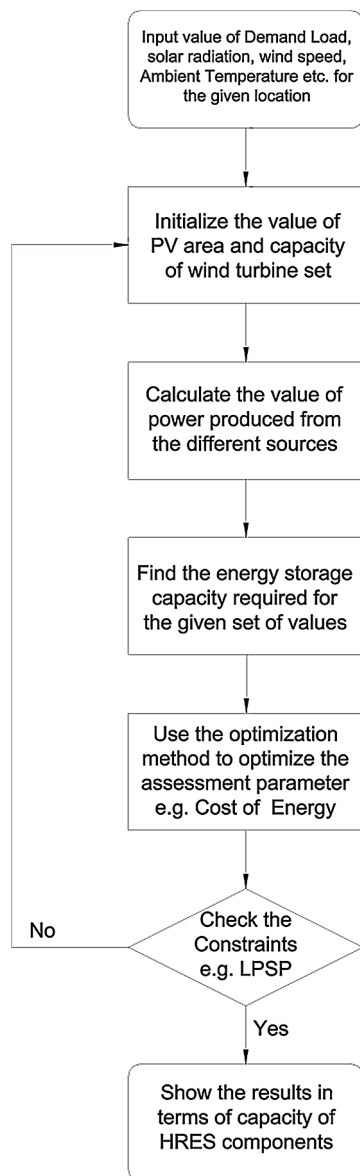


Fig. 2. Flowchart for optimization of solar-wind based hybrid renewable energy system.

of carbon emission, even if there is no carbon emission during the operation of the energy conversion device [24]. An energy conversion device's lifecycle involves mining and transporting raw materials, refining them, and machining and manufacturing the device [25]. These all are energy-intensive operations and hence carbon-emitting. In addition to that, the end of life of these devices requires proper disposal mechanisms. It involves the degradation of the environment [26]. This environmental impact necessitates the analysis of the lifecycle impact of these devices. Several studies are performed to evaluate the overall adverse effects of this equipment on the environment [27]. As per the study [28], 2876 MJ energy is consumed to produce 1 m<sup>2</sup> of the multi-crystalline photovoltaic cell. It is equivalent to 799 kWh of energy. Considering the energy generation by mix coal-fired power stations and others in the energy grid, this can roughly be translated as 663 kg of CO<sub>2</sub>, eq / m<sup>2</sup> of the photovoltaic panel. Baseline Carbon Dioxide Emission Database Version 15.0 [29] by the Central Electricity Authority, Ministry of Power, Government of India, 0.83 kg of CO<sub>2</sub>, eq per kWh, is used to find equivalent carbon emission.

In addition to that, the stagnating economies and increasing automation in the aftermath of the COVID-19 pandemic have increased the

urgency to look for job creation opportunities for policymakers. The renewable sector can boost the demand for the relevant skilled workers and has the potential to offset the job losses in conventional sectors [30]. It also increases the need for adequate training arrangements for the upcoming workforce in the market [31]. Renewable energies are poised to play a significant role in this, and job creation potential needs to be included in the analysis of HRES to evaluate its social impact.

This study uses the Generalized Reduced Gradient (GRG) method for the optimization of the HRES, which is rarely used in the literature for the optimization of HRES [32]. The reliability of the standalone system using the GRG method is performed up to 30 % LPSP. In addition to that, the evaluation of the reliability of the HRES is performed for every 24 hours duration. This daily power loss hours computation ensures that a small annual LPSP doesn't translate into long stretches of the power outage at one go. The grid-connected scenario is also analyzed for both the cases of no payment and with payment from the grid. In addition to that, a new constraint is used for the grid-connected scenario. It limits the amount of energy to be paid for by the grid to the total amount of electricity supplied to the grid. The social impact of HRES is explored in terms of job creation opportunities, which has increased significance in the Post COVID world. The environmental effects of HRES in terms of greenhouse gas emission is also evaluated to compare it with traditional energy extraction methods. The results of the GRG method are compared with the results of HOMER software and are found in good agreement.

The manuscript is structured as following in the upcoming sections. The methodology adopted for the optimal configuration of HRES is described in section 2. It also gives details about the mathematical model adopted in addition to a description of the Generalized Reduced Gradient method. Section 3 describes the remote location selected for the case study, availability of solar and wind resources in addition to demand load profile to be fulfilled. Section 4 details the results and discussion of this study. The results of the standalone case and grid-connected case are described in detail in sub-sections, respectively. Sensitivity analysis is performed and included. The evaluation of environmental and social impact is also presented in subsection 4.4. Sub-section for the validation of GRG results done using HOMER is included after that. The conclusions follow in section 5.

## 2. Methodology

The use of the Generalized Reduced Gradient (GRG) method for the sizing of HRES with the solar photovoltaic, wind turbine, and battery storage systems or grid connection is presented in this study. GRG method is seldom used for HRES sizing. Ladson et al. [32] and Gabriele et al. [33] have compared the GRG method with the other nonlinear programming techniques and have found that GRG has better efficiency and robustness. GRG method is proven to be better than other classical techniques in terms of complexity and computational time, as shown by Rudd et al. [34]. The proposed methodology is simpler to apply and execute. This makes it suitable to be utilized for HRES optimization. Microsoft office 2013 Excel-based add-on "Solver" tool is used to carry out GRG nonlinear method utilization for the optimization process.

A general flowchart of the procedure to be followed for the optimization of HRES is shown in Fig. 2. The case study of the remote rural area is also presented in subsequent sections, where the power demand of several thousand residents of the region is to be fulfilled by the proposed HRES. The purpose is to establish the feasibility of the HRES system optimization using the GRG method.

GRG method uses an implicit elimination method to reduce the decision variables using equality constraints. For instance, an optimization problem has N design variables, K equality constraints and, M inequality constraints. The K equality constraints are used to reduce the number of design variables to N-K variables. This is performed using an explicit method by replacing the dependent variables in the objective function with independent variables using equality constraints. In the implicit method, the problem is solved by combining unconstrained problem

solutions coupled with a root-finding technique [35]. The K dependent variables eliminated from the optimization process are known as basic variables, and the remaining N-K independent variables are known as non-basic variables. In GRG, inequality constraints are handled by introducing a slack variable for each constraint [36]. The HRES components sizing methodology has been carried out using the GRG method. The flowchart representing the GRG method is shown in Fig. 3.

The model adopted for the sizing of HRES is a single objective three variable optimization problem. Solar radiation, ambient temperature, wind speed, and demand load profile are the input to the algorithm in addition to the system component characteristics. Solar radiation and wind speed specify the renewable energy potential of the site at a given time. The load profile defines the power to be satisfied by the HRES. It will also help to quantify any possible deficiency of power.

Component modeling of the HRES is considered as follows [6]. Design variables are the area of PV array,  $A_{PV}$  in  $m^2$ , number of wind turbines,  $N_{WT}$ , and the energy capacity of the battery system,  $E_{BS, max}$  in MWh. Input parameters of the program are hourly load,  $P_L$  for an entire year, solar irradiance,  $I$  for the whole of the year, ambient temperature,

$T$  for the entire year, and wind velocity at reference height,  $V_r$  for the entire year (i.e. 8760 hrs).

The power produced by photovoltaic panels ( $P_{PV}$ ),

$$P_{PV} = \eta_{PV} * A_{PV} * I \tag{1}$$

where,

$A_{PV}$  is the surface area of photovoltaic (PV) panels, in  $m^2$ , it is a design variable.  $I$  is the instantaneous solar radiation, in  $W/m^2$ , it is input data for the location.  $\eta_{PV}$  is the instantaneous efficiency of the photovoltaic panel, it is calculated using Eq. 2.

$$\eta_{PV} = \eta_r * (1 - 0.004 * (T_c - T_{crf})) \tag{2}$$

where,

$\eta_r$  is Rated PV cell efficiency, it is given by the manufacturer of PV panels.  $T_{crf}$  is Cell reference Temperature, it is provided by the manufacturer of PV panels.  $T_c$  is Cell Temperature, it is calculated using Eq. 3.

$$T_c = T + [(NOCT - 20) / 800] * I \tag{3}$$

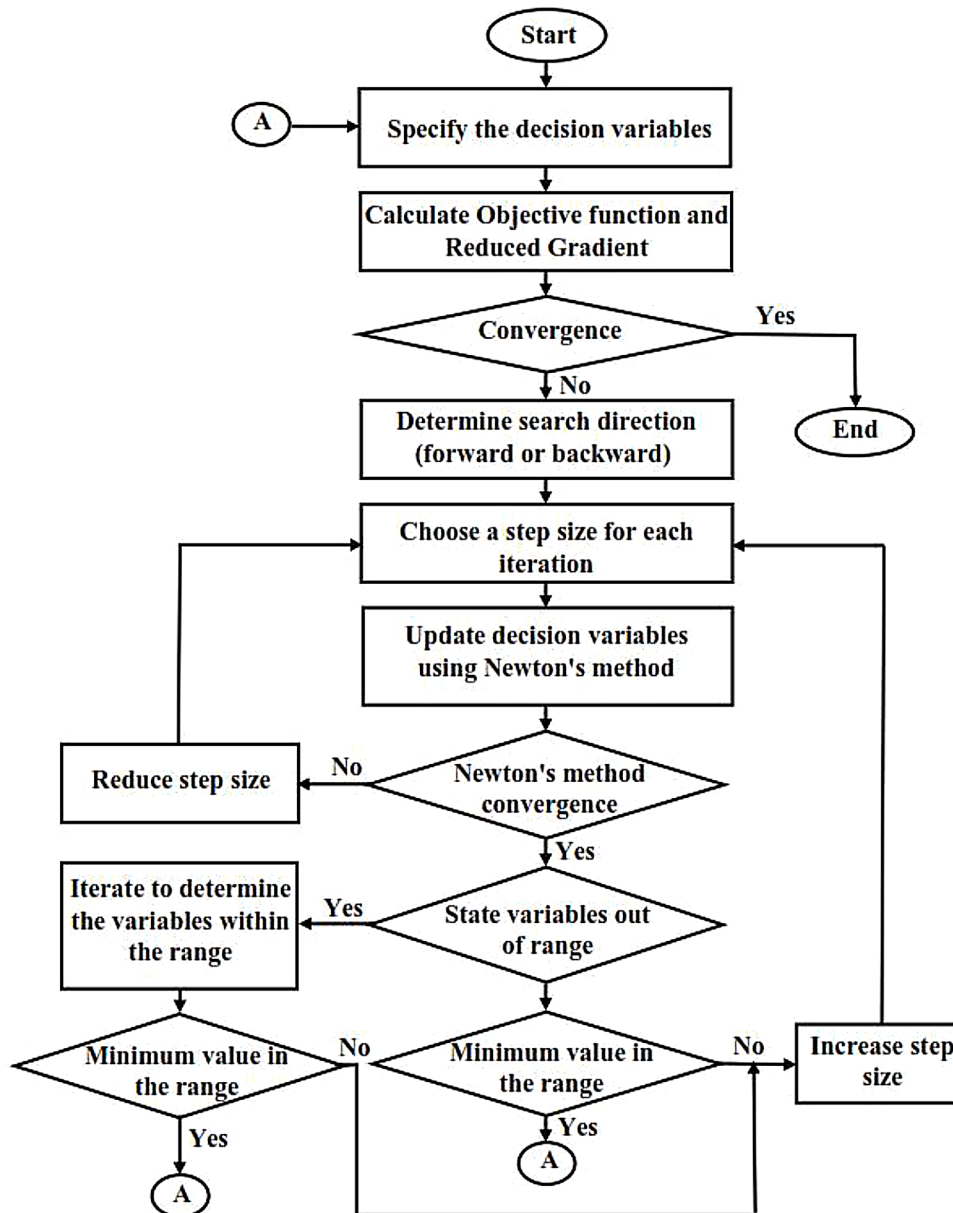


Fig. 3. Flowchart of logical steps of GRG method [37].

Where,

T is the ambient temperature, and it is input data for the location. NOCT (Nominal Operating Cell Temperature) is given by the manufacturer of PV panels. I is the solar Irradiance,  $W/m^2$ , it is input data for the location.

The power produced by the wind turbine,  $P_{WT}$

$$P_{WT} = N_{WT} \times \begin{cases} 0, & v < v_{ci} \text{ or } v > v_{co} \\ P_r \frac{v^3 - v_{ci}^3}{v_r^3 - v_{ci}^3}, & v_{ci} \leq v \leq v_r \\ P_r, & v_r \leq v \leq v_{co} \end{cases} \quad (4)$$

Where,

$N_{WT}$  is the number of wind turbines in HRES, It is a design variable.  $P_r$  is the rated power output of the turbine, in kW or MW, it is given by the manufacturer.  $v_{ci}$  is cut-in wind speed, in m/s, it is the threshold value of wind speed. If wind speed is more than that, the wind turbine will start producing power, which is given by the manufacturer.  $v_r$  is rated wind Speed, in m/s, for the wind speed more than rated wind speed, the wind turbine will produce power as per rated capacity, and it is given by the manufacturer.  $v_{co}$  is cut-out wind speed, in m/s, beyond which wind turbine will be stopped to avoid damage and stop producing power, which is given by the manufacturer.  $v$  is the wind speed at the hub height of the wind turbine, in m/s, it is calculated using Eq. 5.

$$v = v_{rh} \left( \frac{h_{rh}}{h_{hub}} \right) \quad (5)$$

$h_{rh}$  is the reference height, for which wind speed data of location is available.  $h_{hub}$  is hub height of the wind turbine.

Energy interaction with the battery system. State of charge of the battery in terms of stored energy  $E_{BS,t+1}$ , in MWh or kWh, at time step  $t+1$ , is calculated from energy stored in the previous instance  $E_{BS,t}$  at time step,  $t$ ,

$$E_{BS}(t+1) = \max \left\{ \min \left[ E_{BS}(t) + X * \left( \frac{P_L - P_{PV} - P_{WT}}{E_{BS,max}} \right) \right] \right\} \quad (6)$$

Where,

$P_L$  is demand load required to be fulfilled by the HRES, in kW, it is input data for the location.  $P_{PV}$  is power produced by photovoltaic panels at a given instance, calculated using Eq. (1).  $P_{WT}$  is power produced by photovoltaic panels at a given instance, calculated using Eq. (2).  $E_{BS,max}$  is the capacity of the battery, which is a design variable in this optimization problem.  $(P_L - P_{PV} - P_{WT})$  is required power interaction during charging or discharging of battery subject to the maximum state of charge of the battery system  $E_{BS,max}$ .

$X = \eta_{ch}$  for charging and  $X = 1/\eta_{dch}$  for discharging.  $\eta_{ch}$  is charging efficiency of the battery system.  $\eta_{dch}$  is discharging efficiency of the battery system.

Power interaction ( $P_{BS}$ ) of battery system with other components of HRES in a given time period,

$$P_{BS} = E_{BS}(t+1) - E_{BS}(t) \quad (7)$$

The objective function to be minimized is the economic parameter,

$$ALCC = \sum (C_j * Cu_{uj} * CRF_j) + (RoE_{ig} * E_{ig}) - (RoE_{ig} * \min(E_{ig}, E_{ig})) \quad (15)$$

as it is of great concern at the design stage. The economic parameter to be minimized is selected as the levelized cost of energy, as it

encapsulates all the costs incurred to avail a certain amount of power as described in the following equations.

Minimize the objective function, Levelized cost of energy (COE),

$$COE (\$/kWh) = \frac{ALCC (\$/yr)}{\text{Energy utilization (kWh/yr)}} \quad (8)$$

Annualized Life Cycle Cost (ALCC) for a stand-alone system, [38]

$$ALCC = \sum (\text{Cost of components} * CRF \text{ of components})$$

$$ALCC = \sum (C_j * Cu_j * CRF_j) \quad (9)$$

Where j stands for components of HRES i.e. PV, WT or BS. C is the capacity of component, in MW for PV and WT & in MWh for BS.  $C_u$  is the unit cost of the component, in  $\$/MW$  for PV and WT & in  $\$/MWh$  for BS. Capital Recovery Factor (CRF),

$$CRF = \frac{[i * (1+i)^n]}{[(1+i)^n - 1]} \quad (10)$$

where, i, is the internal rate of return and n is the lifetime of the component in years. The value of CRF depends on the lifetime of components and internal rate of return [39,40].

Subject to constraint. Loss of Power Supply Probability (LPSP) [41],

$$LPSP = \frac{\sum LPS}{\sum \text{Total Load in a year}} \quad (11)$$

Where,

$$LPS = \text{Loss of power supply in the given time period (kWh)} \quad (12)$$

When,

Load > Total Renewable Power, Battery discharge happens.

If the battery cannot supply that deficit power due to depletion of its charge, loss of power occurs.

If  $P_{BS} < P_L - P_{PV} - P_{WT}$ ,

Loss of power supply (LPS) occurs and is calculated as,

$$LPS = P_L - P_{PV} - P_{WT} - P_{BS} \quad (13)$$

Where,  $P_L$  is the demand load as an input parameter to computation and  $P_{PV}$ ,  $P_{WT}$ ,  $P_{BS}$  are calculated using Eqs. (1), (4), and (7), respectively.

If  $E_{BS}(t+1) > E_{BS,max}$ ,

Dump Load (DL) is activated when the battery is fully charged, and the total renewable charge is greater than load demand.

$$DL = P_{PV} + P_{WT} - P_L - P_{BS} \quad (14)$$

In addition to the LPSP, which is a well-established reliability criterion [42] for the power systems, additional measures for assessing the system's reliability are also added. The LPSP relates the power losses of the entire year with the load requirement of the entire year for annual timespan consideration. E.g. for the only power loss of 3 consecutive days in a year, the LPSP is less than 1%. But the consecutive power loss of 72 hours may not be acceptable to the users. Looking into this possibility, an investigation of maximum power loss in hours per day (e.g. 8 hours) is done. This will ensure the restriction on consecutive power loss for the consumers on any calendar day.

Annualized life cycle cost (ALCC) for a grid-connected system.  $ALCC = \sum (\text{Cost of components} * CRF \text{ of components}) + \text{cost of power sold to the grid} - \text{cost of power purchased from grid in a year}$

Where, j stands for components of HRES i.e. PV, WT, or BS. C is the

Capacity of the component, in MW for PV and WT & in MWh for BS. Cu is the unit cost of the component, in \$/MW for PV and WT & in \$/MWh for BS.  $RoE_{ig}$  is the rate of energy to be bought from the grid, in \$/kWh.  $E_{ig}$  is the total energy to be outsourced from the grid, in kWh.  $RoE_{ig}$  is the cost at which the power is sold to the grid.  $E_{ig}$  is the total power supplied to the grid. Payment for power supplied to the grid will be restricted to the amount of energy availed from the grid.

The social impact of HRES in terms of job creation is analyzed, as it has become more critical in the wake of pandemic-ridden economies. The components of HRES like photovoltaic panels and wind turbines require adequate investments and employment of suitable people throughout the supply and manufacturing chain [43]. Various studies are published to assess the need for manpower in the manufacturing process, installation of equipment in the plant and operation & maintenance of the systems.

Total job creation is calculated for the respective component of HRES as follows:

Total job creation = Job creation in manufacturing + Job creation in installation + Job creation in operation and maintenance.

$$JC = JC_{man} + JC_{ins} + JC_{o\&m} \quad (16)$$

It has become imperative to evaluate the environmental impact of the HRES system in the context of the looming ecological disaster of global warming and increased awareness in the masses about it. The environmental effects of PV panels can be calculated from the optimal area of PV calculated earlier. The increasing reliability requires a higher capacity of PV and in turn higher share of embodied carbon. In the same way, quite a variation is observed in the studies of life cycle analysis examining the environmental impact of wind turbines from the cradle to the grave. Crawford [44] suggested embodied carbon in the wind turbines in the range of 1844–2074 tons of CO<sub>2,eq</sub> per MW of capacity. Wang et al. [45] demonstrated that the value is 1664 t, CO<sub>2,eq</sub> per MW. Guezuraga et al. [46] reported the range of 1037 – 2292 t,CO<sub>2,eq</sub> per MW.

Annualized Embodied Carbon (AEC) (in tons of CO<sub>2</sub> equivalent/year) = Total lifecycle embodied emission (in tons of CO<sub>2</sub> equivalent) / life of component (in years)

$$AEC = \frac{TEE}{n} \quad (17)$$

### 3. Case study

The GRG method described in section 2 is utilized for the case study of a site in India. The study considers a rural area, Jakhau (23°13'07"N, 68°43'01"E), in the west part of the Gujarat state of India. This region is one of the least rain receiving areas and thereby not vibrant in terms of agriculture and livestock (pastoral) cultivation, the two dominant traditional livelihood means. There are instances of entire monsoons without any rain. This has led to accumulated economic backwardness in the region [47]. The area is blessed with one of the highest renewable potentials in terms of solar radiation and wind speed.

This particular area's identification and selection are due to its economic backwardness coupled with relatively higher renewable potential. Sixty-two potentially backward regions were identified through the length and breadth of the state. They include two or more sites explored in each district of the state. The solar and wind potential was gathered for all these sites. Jakhau comes out as one of the sites with the highest cumulative renewable energy potential.

Location of the region near the tropic of cancer and ocean coast along with a large part of the year with a clear sky provides the opportunity to exploit solar and wind energy to develop the area and improve the lives of the region's people. In addition to that, the temporal complementarity of solar and wind potential with load shows the prima facie feasibility of the HRES system installation. The solar radiation data, acquired from the National Solar Radiation Database (NSRDB), shows relatively lower

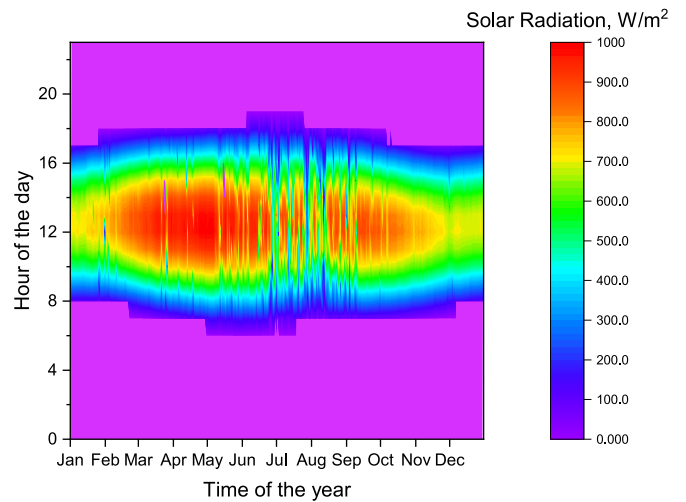


Fig. 4. Solar radiation hourly profile for typical meteorological year.

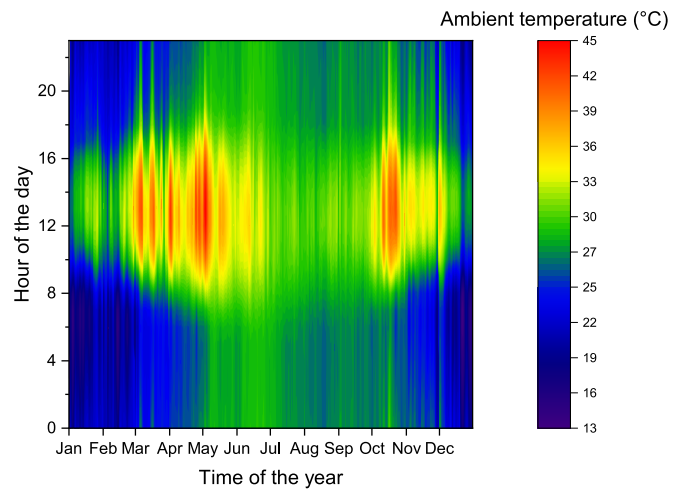


Fig. 5. the temperature profile of all the days of the year.

solar radiation availability in the monsoon season [48]. Fig. 4 shows the hourly solar radiation profile of the entire year. No of hour indicated here onwards starts from 1st January and progresses through the

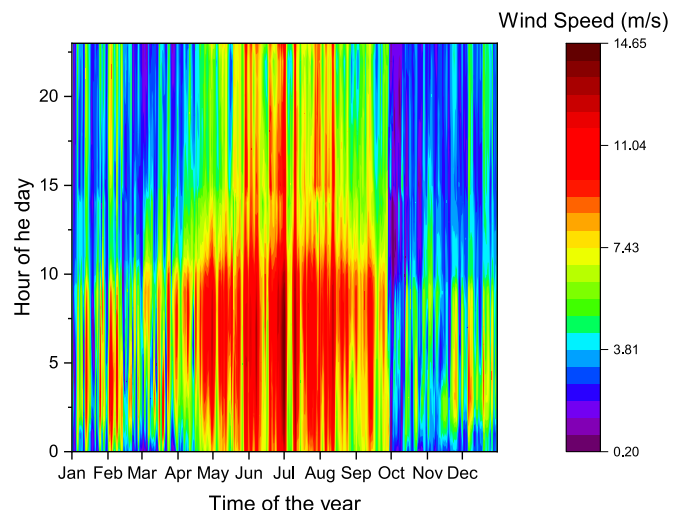


Fig. 6. Wind speed variation through the year at 50 m height.

calendar year. As evident from Fig. 4, the highest solar radiation is received in April and May, and so the highest temperature as shown in Fig. 5. The 1 hour time step is selected for the simulation. That results in the depiction of solar radiation in the morning and evening for all the days with sunrise and sunset in that hour.

The period of a quarter of the year from October to February is winter in this part of the world. In this period, the temperature recedes to near 10 °C levels, and generally, it is the dry season. The following four months are considered the summer. This part of the year has high sunshine available and part of it has good wind potential as well.

July to October is considered monsoon season, which brings in precipitation by the south-westerly winds. So this provides good periods of relatively high wind speeds, as evident from Fig. 6. But due to clouds, the solar radiation is not consistent and reliable. July and August, which lie in the monsoon season, have the least solar radiation available. In contrast, March and April have maximum solar potential.

Wind potential available in the May to August period is highest because of monsoon winds. That also roughly coincides with higher load demand in the period of March to Jun as shown in the daily load profile in Fig. 7. On the other hand, November and December see the lowest wind speeds. Parameters chosen for the simulation of HRES are shown in Table 1.

The data of 8760 hours of the entire year for solar radiation, wind speed, and ambient temperature are available for the location, derived from the NSRDB [49]. The hourly values of the entire year are considered for computation. The load data is from the state load dispatch center [50], which facilitates smooth and reliable grid operations, including short-term demand forecast to absorb the renewable power into the grid better. The power-law coefficient for adjusting wind speed at hub height is 1/7, as the terrain is mainly flat [51].

The solar radiation, ambient temperature, wind speed, and demand load of all 8760 hours was fed into the program to compute the sizing of HRES components. Two types of scenarios are considered solar PV and wind turbine hybrid systems. Scenario A is the system working in standalone mode, and Scenario B is the grid-connected scenario without a battery system.

In scenario A, computation of solar energy is done using instantaneous efficiency of photovoltaic panels for given ambient temperature and solar radiation at a given time as described. The wind speed is adjusted for the hub height elevation using power law. In addition to that difference between load and renewable power produced is calculated. If renewable power is more than load and the battery is not fully charged, the power will go to the battery, and if the battery is completely charged, the power will go to the dump load. When renewable power is

**Table 1**

Parameters considered for the computation [39,52–54].

Parameter	Value	Parameter	Value
Internal rate of return	12%	Life of Wind Turbine	20 years
Life of Photovoltaic panels	20 years	Hub height	50 m
Cell reference Temperature	25 °C	Power law coefficient	1/7
Nominal Operating Cell Temperature	45 °C	Cut-in wind speed	3 m s <sup>-1</sup>
Rated PV cell efficiency	16%	Rated wind Speed	13 m s <sup>-1</sup>
Life of Battery Systems	5 years	Cut-out wind speed	25 m s <sup>-1</sup>

less than the demand load, the battery will supply deficit power and get discharged. If the battery is fully discharged and the power deficit remains, the instance is counted as the loss of power supply. This total demand, which is not met in the instances of the loss of power supply, is used to find the loss of power supply probability (LPSP). The constraints fed to the optimization process are the LPSP value and integer value of the number of wind turbines. The optimized values of the photovoltaic panel area, no. of the wind turbine, and capacity of the battery system are decision variables as the results of optimization process. The capital cost of the components and their CRF gives the annual life cycle cost (ALCC). The useful energy produced by the plant can be used to find the Cost of Energy (COE) per kWh. The LPSP is changed gradually, and its effect on the COE is observed.

For the grid-connected scenario without a battery system of scenario B, the gap between renewable power generated by the solar photovoltaic panels and wind turbines is filled by the grid. When renewable power is greater than the load demand, surplus power is supplied to the grid. In the case of the deficit supply from renewables, the remaining load power is drawn from the grid. This scenario can lead to several possible cases. When the grid operator follows the policy of not paying anything to HRES owners in exchange for the electricity supplied to the grid, there is no economic gain in supplying electricity to the grid. When the grid operator pays some contracted price for the power supplied from the HRES, the ALCC of the plant will decrease that much. Different prices being paid for this supply are considered for the results of a range of possibilities worth mentioning. In addition to that, the grid operator may charge the rate of electricity drawn from the grid at the deficit times not favorably to HRES. This also has the potential to many different sub-scenarios, which are discussed in the results section.

## 4. Results and discussion

### 4.1. Scenario A: Stand-alone system with photovoltaic panels, wind turbine and battery system

Standalone system of solar photovoltaic, wind turbine, and battery system based HRES is sized for the site mentioned in section 2 with the methodology described in section 3. This scenario A is implemented and simulated for the varying values of LPSP. The results of the simulations are shown in Fig. 8.

Each of these COE values is the optimal value corresponding to optimal sizes of components for given constraints and situations among the values computed by the round of simulations. Increasing LPSP means the decreasing reliability of the system and an increasing amount of load will remain unfulfilled. The zero value of LPSP indicates a completely reliable system for supplying all load as simulated by the power generation formulas and input data.

The increase in the LPSP gives a substantial drop in the COE of the systems, especially for initial values, as shown in Fig. 8. This indicates that if the loss of load for that tiny period is tolerable, the gain in economic terms is markedly high. The dump load inches downward at 2% LPSP. It does not decrease much with an increase in LPSP at higher LPSP values. The 98% reliable system seems to be preferable provided the consumers are willing to take power cut for the 2% of load [55], as it

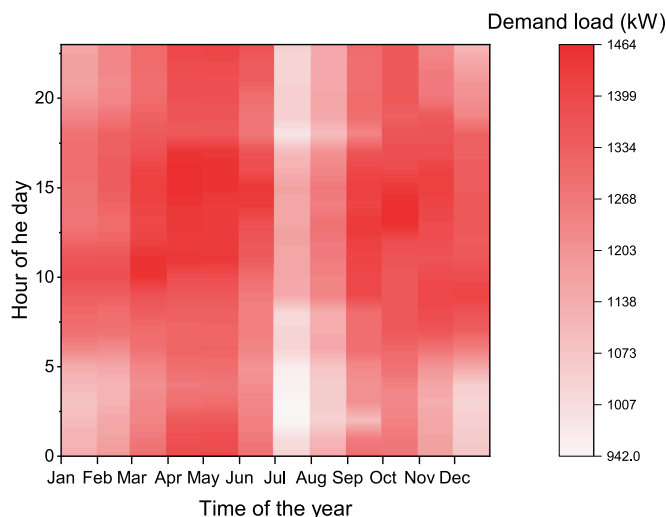


**Fig. 7.** Monthly average daily demand load profile.

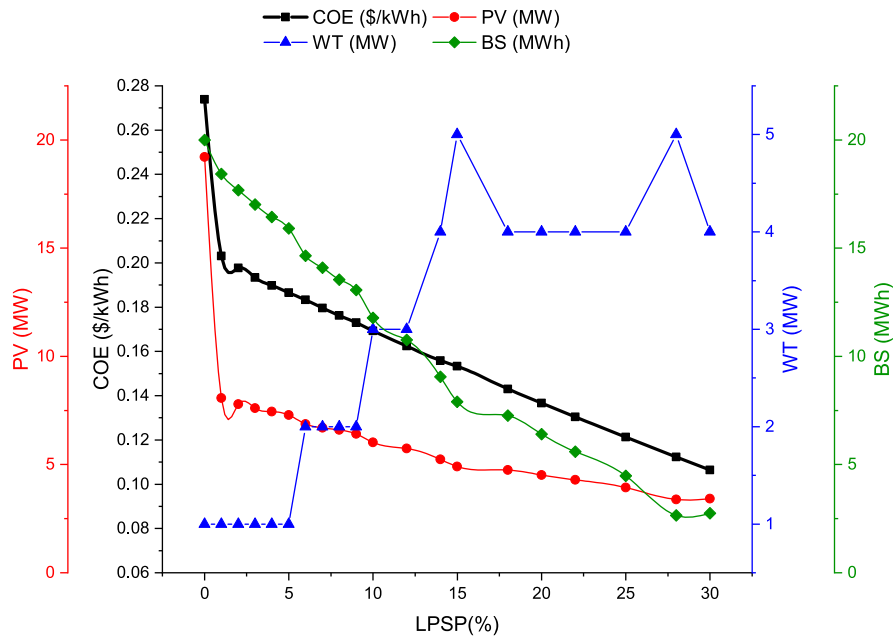


Fig. 8. Optimal configuration of the standalone system for different reliability levels.

provides a reasonable trade-off in component sizes, COE and dump load. The dump load is with respect to the total load satisfied by the system. This load is a wastage of energy due to the temporal mismatch between high load demand and high renewable supply periods.

The completely reliable system requires the aid of a wind turbine and high battery capacity in addition to high PV capacity, as it requires a higher capacity of the wind turbine to fulfill the demand completely in the absence of sunshine. Then with an initial increase of LPSP, wind turbine retains lower capacity, as shown in Fig. 8 because those tiny power losses are now tolerable for lower reliability. Unlike solar PV capacity, the wind turbine is rated in the multiple 1 MW only. For LPSP more than 5, the capacity of the wind turbine increases and becomes comparable to PV capacity at the expense of reliability. This happens owing to the fact that the complementary nature of solar and wind comes into play and reduces the battery storage requirement. Energy, which goes into loss of power supply instances. The simulation selects 5 MW capacity for 15% and 28% LPSP because the LCOE with 4 MW wind

turbine capacity is slightly higher. It happens due to the incremental loss of power supply in times of good wind power availability, which is better served by wind turbines.

As shown in Fig. 9, for the case of zero LPSP, the total power produced by the PV and WT has a mismatch with the load requirements at some times. This necessitates the battery to satisfy the load at deficit times. Some days in the year leave the net deficit of the power due to lower renewable availability, as shown in Fig. 9. This period will require a larger battery capacity than just to fulfill the arbitrage of the day. This necessity of a lot of accumulated charge in the battery increases the battery capacity requirements a lot. This is especially true for the high-reliability cases with very low LPSP. Suppose some loss of load is acceptable to the consumers in periods with relatively low renewable potential. In that case, a significant drop in the battery capacity can be achieved, resulting in lower COE.

An additional approach to reliability is explored in this study. The LPSP gives average power failure hours in an entire year, which may

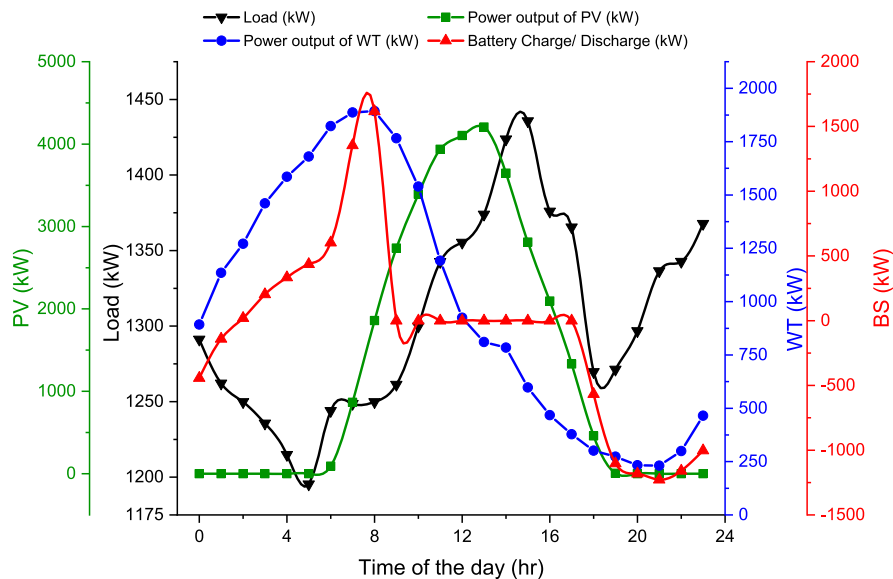


Fig. 9. Sample of a day (June 1) for component power interactions for LPSP 0.

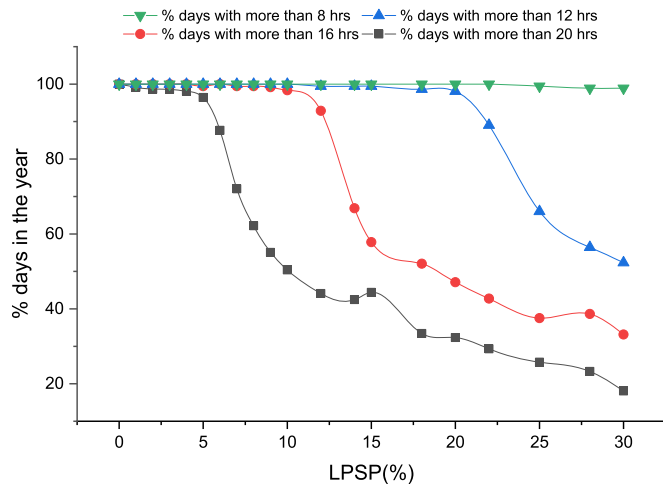


Fig. 10. No. of days with power availability hours in a day for different LPSP.

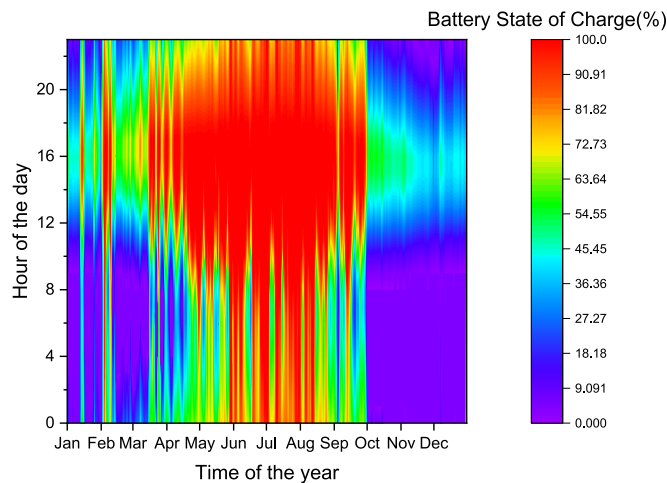


Fig. 11. Battery state of charge throughout the year.

result in continuous power loss concentrated for a certain period of time. This may result in small LPSP with long power loss hours in a certain section of the annum. To study this probability, the computation of power loss hours for all the days of the year is performed. As shown in Fig. 10, no. of days with power loss in the limit of 4 hours, 8 hours, 12 hours, and 16 hours are plotted. It reveals that for LPSP up to 20%, very few days with a large number of power loss hours are observed and the problem of continuous power supply for a certain period doesn't occur.

A higher share of the battery system in levelized cost of energy leads to further investigation of the battery system sizing. Fig. 11 shows the state of charge of the battery for the entire year. It reveals that the discharge of the battery in times of higher wind potential in monsoon is low. Fig. 11 shows the battery charge condition for a thoroughly reliable system.

#### 4.2. Scenario B: Grid-connected system with photovoltaic panels and wind turbine

The policy of facilitation of grid-connected HRES can be the way forward to promote renewable energy sources and maintain the reliability of the HRES. The grid-connected system of scenario B has no battery system available at its disposal, so the difference between renewable power and the load is filled with grid interaction. This leads to a question of the arrangement of electricity pricing with the grid. The question of energy pricing is twofold: cost of purchase of electricity from

the grid and sell price of electricity to the grid.

The two cases for scenario B of grid-connected HRES are simulated. The two cases are for 2 different arrangements regarding the sale price to the grid [56–58]. The first case I is with respect to no payment by the grid to the HRES for energy supplied to the grid. Case II is for the sale price of 0.029 \$/kWh (2 ₹/kWh) for the electricity supplied to the grid. This is to investigate the effect of the sale price on the optimal configuration of grid-connected HRES.

The cost of electricity available from the grid varies from 0.043 \$/kWh (3 ₹/kWh) up to 0.214 \$/kWh (15 ₹/kWh). The pricing variation is explored to get a better idea of the feasibility of the HRES plant. Additionally, the cost of purchase of electricity will depend on the agreement by the HRES owners with grid operators and distribution companies. This is affected by the comfort of the grid operator to provide power at the time of renewable deficits [59]. Generally, at these times, the grid will already be running its peaker plants. The peaker plants are costly to run in comparison to the base plants. The cost of the electricity derived by the grid operator is likely to cost more than regular prices. This fact has led to consider the purchase cost up to 0.214 \$/kWh (15 ₹/kWh). The government may adopt the policy of low price of the purchase from the grid to promote the HRES installations. That's why the lower purchase prices are also considered for the analysis.

##### 4.2.1. Case I: Grid-connected system with no payment for the supply to the grid

The simulation results of scenario B computations, for the case I, are summarized in Fig. 12. The electricity purchase cost at deficit times from the grid is varied, and its effect on the HRES sizing and power interaction is analyzed. Purchase cost variation is from 0.043 \$/kWh (3 ₹/kWh) up to 0.214 \$/kWh (15 ₹/kWh).

The wind turbine is not in the optimal mix at a very low purchase price from the grid, as evident from Fig. 12. The detailed analysis of power interaction reveals that the higher plant load factor of solar PV causes the HRES to draw power from the grid in the absence of sunshine instead of opting for the wind turbine to minimize the levelized cost of energy.

Wind turbine comes in the optimal mix bit late, but increases the capacity rather rapidly and crosses the PV in capacity at the price of 0.171 \$/kWh. The rapid increase in the WT capacity is due to its ability to provide power besides the sunshine hours. The increasing cost of purchase power tends to decrease the dependence of the HRES on the grid, as evident in Fig. 12, to decrease the outgo of money to the grid.

The levelized cost of energy steadily increases with purchase cost, but the difference between the two grows as observed in Fig. 12. The COE at a purchase cost of 0.043 \$/kWh is 0.040 \$/kWh, which increases to 0.143 \$/kWh at purchase cost 0.086 \$/kWh. It is evident that an increase in COE is not as profound as an increase in the purchase cost. This results from the increased share of renewables that replaces grid electricity, as evident in Fig. 12. As the price of purchase increases, the power drawn from the grid decreases steadily, as shown in Fig. 12. At the same time, the power supplied to the grid increases substantially as there is an increase in the Fig. 12 capacity of PV and WT to decrease the increasingly costly power drawn from the grid. The electricity supplied to the grid becomes larger than the electricity received at a higher purchase cost is due to the same reason, as also observable in Fig. 12.

##### 4.2.2. Case II: 0.029 \$/kWh sale price to the grid

It is crucial to consider the effect of the sale price to the grid on the optimal configuration of grid-connected HRES. This case considers the sale price of 0.029 \$/kWh to the grid for variation of the purchase price from 0.043 \$/kWh to 0.214 \$/kWh.

The sizing optimization results of case II reveal that PV and WT both increase their size for low purchase cost until a particular value of purchase cost as shown in Fig. 13. This is unlike previous cases, where PV size was on the secular decline. This can be explained by the increased incentive to the system for power sale compared to the

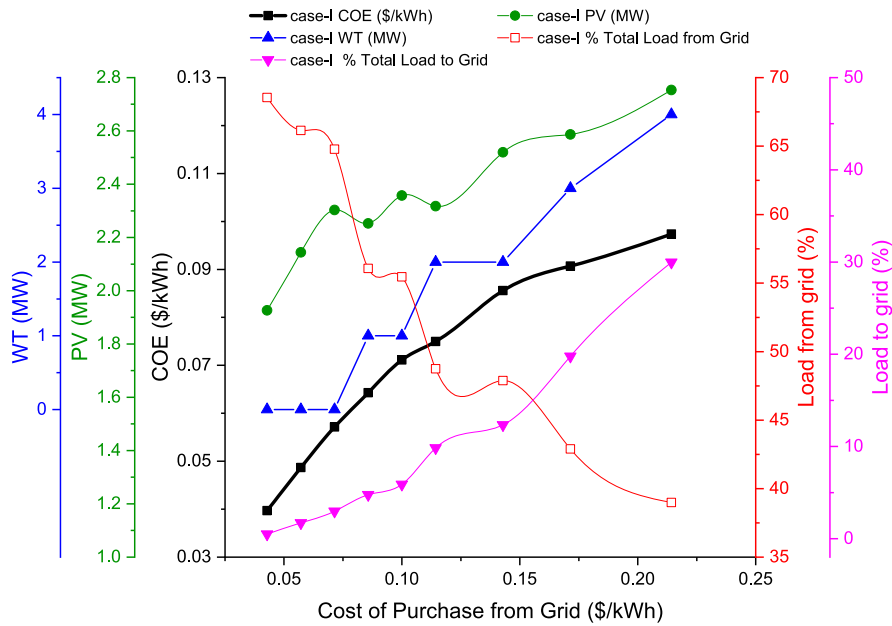


Fig. 12. Optimal configuration of Case-I in grid-connected scenario.

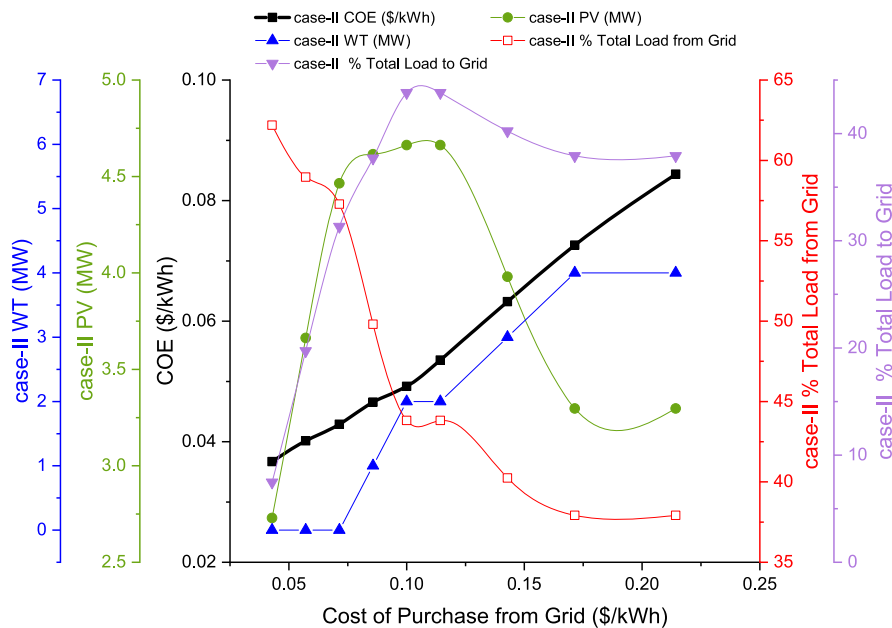


Fig. 13. Optimization results for case-II for component sizing and grid interaction.

previous case due to increased sale price. Otherwise, the general trend can be attributed to the same factors as was in previous cases.

A large amount of electricity is drawn at low purchase prices. The amount of electricity supplied to the grid quickly matches the decreasing load derived from the grid, as shown in Fig. 13. This is the result of increased effort from HRES to minimize the load acquired from the grid at a high purchase cost.

#### 4.2.3. Comparison of grid-connected cases

As mentioned earlier, the comparison of all cases can have important insights, which can broaden the perspective regarding the HRES sizing for different grid-connected price mechanisms. This can have policy implications as well.

The photovoltaic panel capacities start low and increase a bit with an increase in the purchase price for the first case I, as evident from Fig. 14.

Case II is a bit like a transition case where PV increases, peaks, and decreases at higher purchase costs. Interestingly enough, the weight of PV in total ALCC of HRES (including PV annualized cost, WT cost, grid purchase and sale in a year), remains the same for all purchase prices and both cases. This can be due to the arrangement of load distribution with respect to solar availability in such a manner that despite the change in the size of PV (capacity, MW) for different cases and sub-cases, it retains its % share (normalized weight) in COE at the same level on an annualized basis.

The wind turbines don't get added in the optimal mix at a very low purchase price from the grid for both cases, as evident from Fig. 14. This is due to the availability of electricity from the grid at a low cost at times of absence of sunshine and not very consistent wind power availability. This is also because of a cubical decline in wind power in comparison to a linear decrease of solar power at less than rated wind speed. Higher

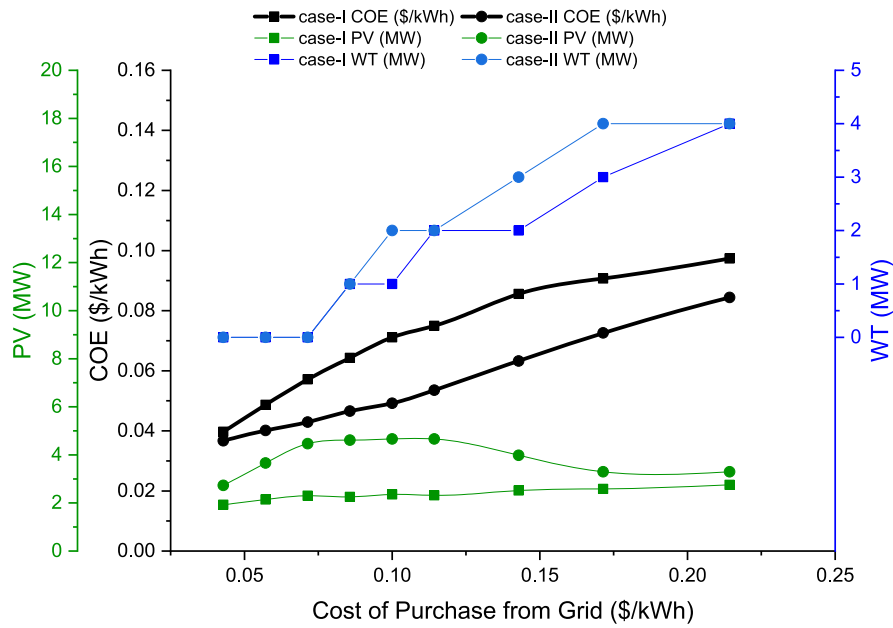


Fig. 14. Comparison of optimal configuration of grid-connected cases.

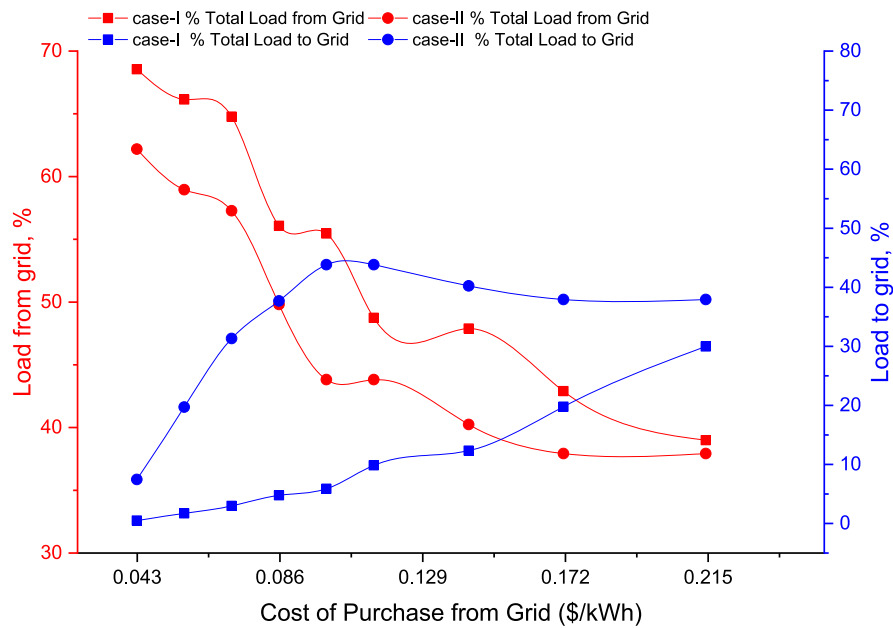


Fig. 15. Comparison of energy interaction with the grid for both the cases.

purchase cost demands higher wind capacity to replace the costly purchase of grid power at night times for all cases. This also leads to an increase in the weight of wind turbine cost in the COE at the expense of grid payment share.

The levelized cost of energy variation profile remains essentially the same for different cases except for minute subtraction at higher sale prices, as seen in Fig. 15. Total load derived from the grid shows a secular decline for all the cases with increased purchase cost from the high 60 s to low 30 s in terms of percent of total load demand on the HRES.

#### 4.3. Sensitivity analysis

The effect of variation of different input parameters on the levelized cost of energy extracted from HRES needs to be investigated because it

will ascertain the effect of market forces and other external factors on the feasibility of HRES. The effect of change in the capital cost of HRES components namely PV, WT, and BS on the cost of electricity, is shown in Fig. 16. It reveals that COE is highly sensitive to battery cost. This increases hopes for the decreasing battery cost for the better economic viability of HRES in the near future.

The effect of variation in component cost on the COE will also depend on the relative share of components in the system among other things. That's why the case-specific sensitivity is shown in Fig. 16. The change in the rate of return is more on the annualized cost of PV and WT compared to the annualized cost of BS owing to the former's long lifetime. The sensitivity analysis reveals that increasing technological advances in the manufacturing of PV [60], WT [61], and BS [62] coupled with low-interest scenario [63] going forward is poised to improve the economic viability down the line. The effect of change in solar radiation

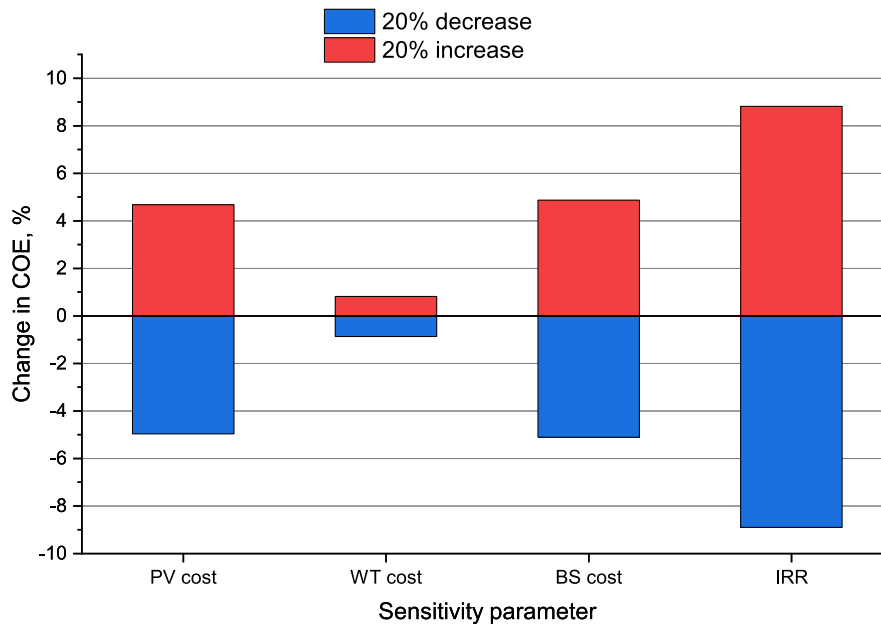


Fig. 16. Sensitivity of HRES COE with respect to component cost and IRR.

does not result in differences in the sizes of PV components and by the extension to COE.

4.4. Environmental and social impact of HRES

The economic slowdown in the wake COVID-19 pandemic makes it much more imperative to think about the growing unemployment rates throughout the different parts of the world [64]. Lower GHG emissions made it possible to see clear blue skies in many cities of the world [65]. Policymakers are increasingly looking for the ways to provide the stimulus packages in such a way that they can stop the downhill slide of economies. In addition to that, policymakers have a window of opportunity to make structural changes so that it can also create long-term societal and environmental benefits. Investment in renewable energy sources is pretty beneficial in terms of job creation and giving respite

from carbon-emitting sources. The green deal [66] announced by European Union authorities is worthy of mention at this juncture.

4.4.1. Carbon emission calculation

The environmental effects of PV panels can be calculated from the optimal area of PV calculated earlier. The increasing reliability requires a higher capacity of PV and, in turn higher share of embodied carbon. In the same way, quite a variation is observed in life cycle analysis studies examining the negative environmental impact of wind turbines from the cradle to the grave. Crawford [44] suggested embodied carbon in the wind turbines in the range of 1844–2074 tons of CO<sub>2,eq</sub> per MW of capacity. Wang et al. [45] demonstrated that the value is 1664 t,CO<sub>2,eq</sub> per MW. Guezuraga et al. [46] reported the range of 1037 – 2292 t,CO<sub>2,eq</sub> per MW.

Annualized embodied carbon in the components of HRES is depicted

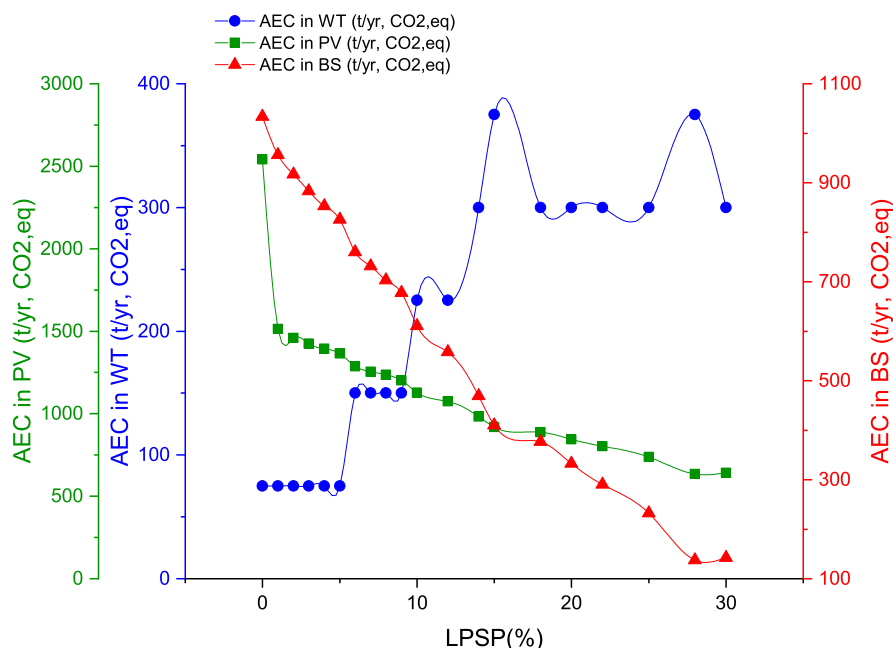


Fig. 17. Annualized embodied carbon (AEC) in HRES components in standalone scenario.

in Fig. 17. The PV is responsible for a higher share of GHG emissions in comparison to other components because it has a higher share in terms of capacity in optimal configurations of HRES. At lower reliability levels, the reduced capacity of PV decreases the difference between embodied carbon of different components of HRES.

It is all the more important to investigate the amount of GHG emission prevented due to the installation of HRES compared to the grid connection, where conventional sources still play a dominant role in the energy mix. The difference between the total of AEC of all the components of HRES and carbon emission for equivalent energy availed from the grid gives the total emission decrease. The benefit to the environment is significant, as shown in Fig. 18. The carbon footprint per unit of energy consumed is also depicted here. If all the energy produced by the HRES is taken into account, the carbon footprint will be even less.

The negative environmental impact of the grid-connected scenario is investigated as shown in Fig. 19. However, it is better in terms of economics in comparison to a standalone system. The total annual carbon emission and reduction in complete grid dependence show a substantial reduction in harm to the environment, albeit less environment friendly compared to standalone systems. This is the trade-off to be made by the decision-maker between the two. An increase in the carbon emission, in this case, is since the portion of power demand satisfied by the grid is added in the calculation of AEC in addition to the HRES component life cycle emissions, which is the major chunk of the total AEC. The increase in the purchase price of power from the grid induces the higher capacity of HRES and decreases its dependence on the grid. It results in higher renewable share and better environmental friendliness for higher purchase cost, as evident in Fig. 19.

4.4.2. Job creation

The components of HRES like photovoltaic and wind turbines require adequate investments and employment of suitable people throughout the supply and manufacturing chain [43]. Various studies are published to assess the need for human resources in the manufacturing process, equipment installation in the plant, and operation & maintenance of the systems.

The jobs created by PV components at the manufacturing and installation stages are higher in comparison to others. This is because PV requires more power at this stage and its higher share of capacity in the HRES system.

Summary of total jobs created by the different components of HRES,

as shown in Fig. 20, affirm that employment opportunities offered by the PV are one order of magnitude higher in our specific study for the reasons mentioned earlier. The study firmly establishes the opportunities for the skilled workers of different strata in the growing hybrid renewable sector.

In the same way, the grid-connected scenario of HRES, as shown in Fig. 21, also provides job opportunities albeit less than the standalone case as scenario B has smaller component sizes compared to scenario A.

4.5. Validation

The optimal configuration of HRES is found using the GRG method in this study. It is pertinent to validate the methodology adopted by comparing its results with the well-established algorithm. All of the scenarios and cases of this studied are also simulated in the HOMER with the same input parameters to validate the method's robustness [67]. The HOMER was originally developed by National Renewable Energy Laboratory (NREL), USA [68]. It is recognized as standard software to model and analyze hybrid renewable energy systems in this software. Many studies are published wherein the HOMER is used to simulate and optimize HRES [69]. Das et al. have used HOMER to optimize the sizing and the cycle strategy of HRES for the location in Australia [70]. Khan et al. [71] have found the optimal configuration of HRES for four different locations in India using HOMER. Zahboune et al. [72] have used HOMER to compare it with their proposed method for the optimization of HRES. Jufri et al. [73], Zahboune et al. [74], Al Sharafi et al. [75], Amrollahi et al. [76] have validated their optimization modeling of HRES using HOMER.

The input parameters to HOMER were the time series data of solar radiation, wind speed, temperature, and demand load of 8760 hours of the entire year. These were the same for the GRG simulation. The results of HOMER and GRG for the standalone scenario are compared in Fig. 22. It shows the proximity of results of COE of HOMER and GRG method and thus validates the methodology adopted in this study. The difference in results of GRG and HOMER varies from 0.005 to 0.021 \$/kWh and narrows down for the higher LPSP. The small difference in the COE of HOMER results compared to GRG results is that HOMER relies more on PV, whereas GRG is more reliant on BS, as is evident from Fig. 22.

The variations for the component sizes are also tiny. For PV, the HOMER computations result in higher PV capacity than GRG results in the range of 0.04–0.8 MW and for BS, GRG results give higher BS

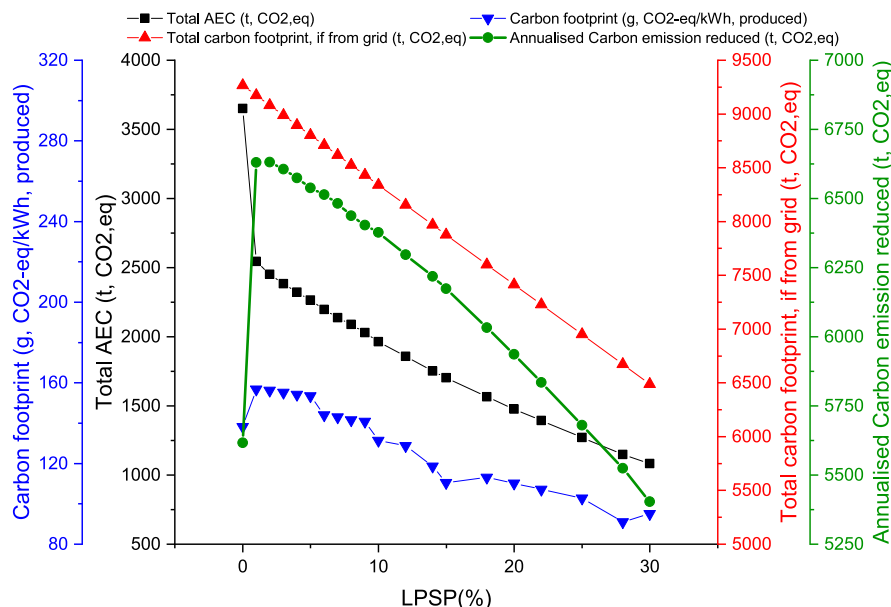


Fig. 18. Comparison of standalone system with conventional sources and decrease in environmental impact.

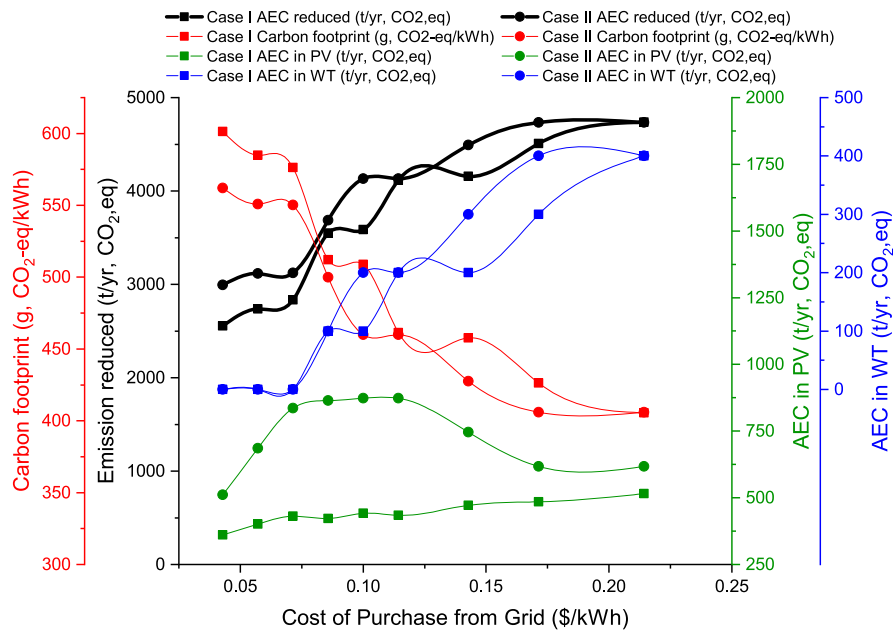


Fig. 19. Negative environmental impact of the grid-connected scenario.

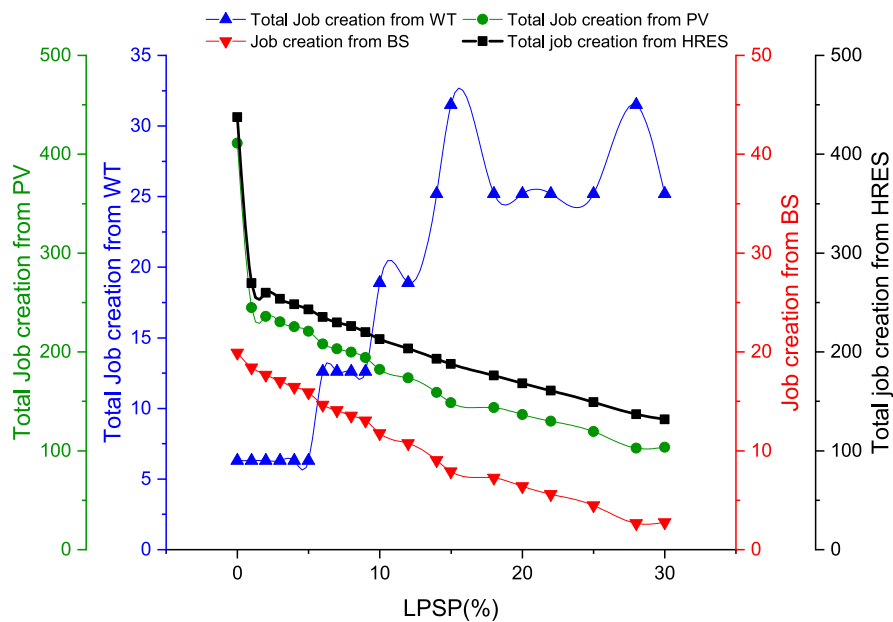


Fig. 20. Job creation opportunities in standalone scenario.

capacity than HOMER in the range of 0.3–2.2 MWh. PV and BS compensated for each other in that way. It seems that HOMER prefers power source availability over energy storage devices.

For the grid-connected scenario, the HOMER simulation for the same input parameters and component characteristics also validates the usefulness of GRG for the optimal configuration of HRES. Fig. 23 summarises the results of sizing of components and economic parameters of HOMER compared to the GRG results. It is evident that GRG performs well in finding optimal PV and WT capacity and minimum COE value for this scenario.

In general, both methods give fairly similar results. The difference between the modified GRG results and HOMER range in 0.000–0.002 \$/kWh in the case-I of grid-connected scenario. PV capacity is more in the GRG results in the range of 0.04–0.13 MW. The capacity of WT remains almost the same except for the transition case, when HOMER is

trying to be less reliant on the grid. Reliance on the grid in both, GRG and HOMER, remains the same, with deviation in the range of 1.66–4.54%.

The results of HOMER simulations for grid-connected case-II are compared with the results of GRG as plotted in Fig. 24. COE in both GRG and HOMER is almost exactly the same at lower purchase prices. The deviation is minimal in the range of 0.001–0.008 \$/kWh. The similarity in results of HOMER and GRG in size of PV and WT show a similar trend to the previous case-I. Thus, the GRG is validated in this case also.

Thus, the GRG is validated with reference to HOMER for all the cases and is performing very well in finding out the best economic parameters.

### 5. Conclusions

The optimal configuration of the hybrid renewable energy system is

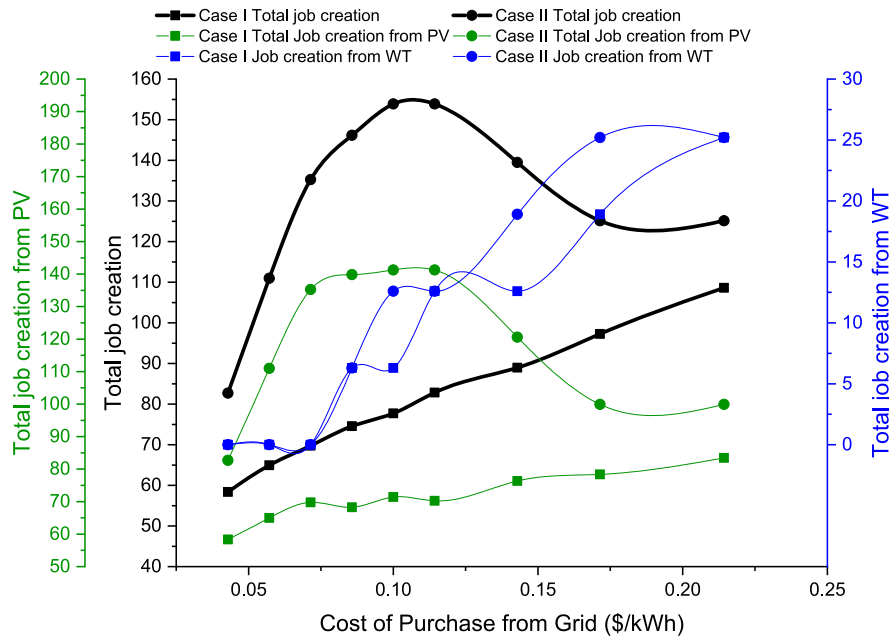


Fig. 21. Job creation in grid-connected scenario.

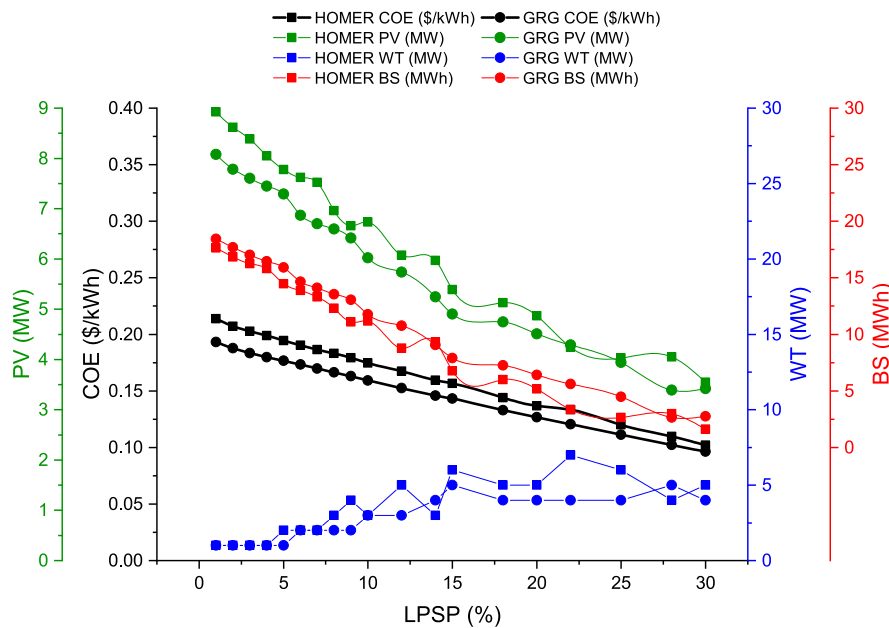


Fig. 22. Comparison of GRG results with HOMER results for standalone scenario.

presented using the generalized reduced gradient method. The renewable energies of solar photovoltaic panels and wind turbines are augmented with battery energy storage and grid-connected system in two different scenarios. The COE of standalone HRES ranges from 0.096 \$/kWh to 0.23 \$/kWh for 70% to 100% for different reliability levels. Battery storage has a major share in the cost of energy especially for high-reliability standalone cases and thus higher sensitivity of COE for the cost of the battery storage system. The grid connection can improve the economics of HRES in a big way. The electricity sale price to the grid of 0 \$/kWh (no payment of electricity supplied to the grid) and 0.029 \$/kWh is considered for the computations as case-I and case-II. Both cases are investigated from the grid purchase range from 0.043–0.214 \$/kWh. The COE is in the range of 0.040–0.097 \$/kWh and 0.037–0.084 \$/kWh for case-I and case-II, respectively. The optimization results show

that the grid sale price affects the component sizes of HRES, especially at low purchase cost and overall COE. The GHG emissions from the life-cycle of different components of HRES are also studied. It is predicted that HRES can reduce the GHG emissions in the range of 5.4–6.6 million kg of CO<sub>2</sub> equivalent every year compared to grid power in the standalone scenario. In addition to that, the calculation of employment opportunities shows hundreds of jobs created by the installation of HRES. The methodology validation is done by comparing its results with the results of the HOMER software, which closely matches. The extensive study of the sizing of HRES with a case study shows that the standalone system is better for sustainability and job creation. In contrast, the grid-connected system is better in terms of reliability and economics. The multi regression analysis can be used in the future to develop the relationship between different parameters of the battery.

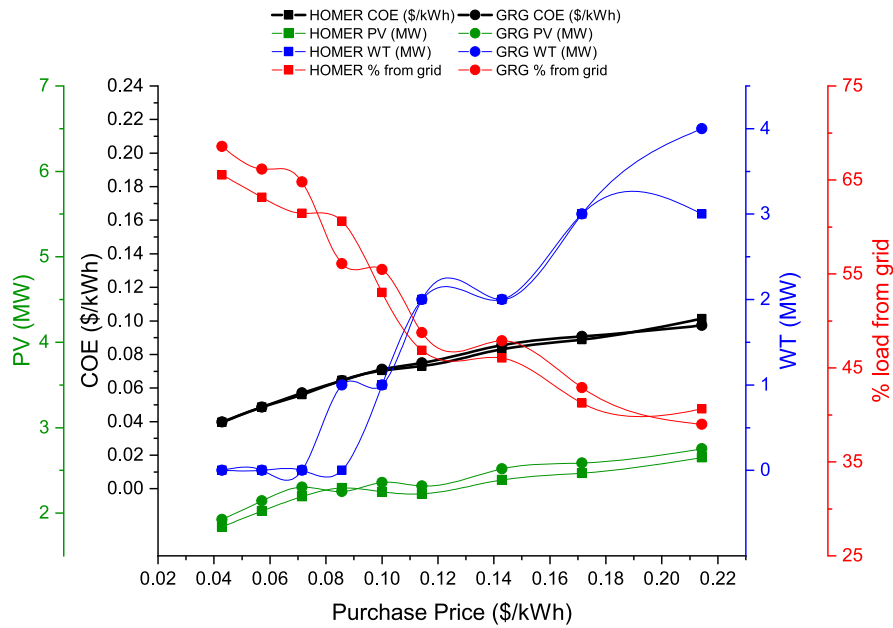


Fig. 23. validation of results for case-I of grid-connected scenario with HOMER results.

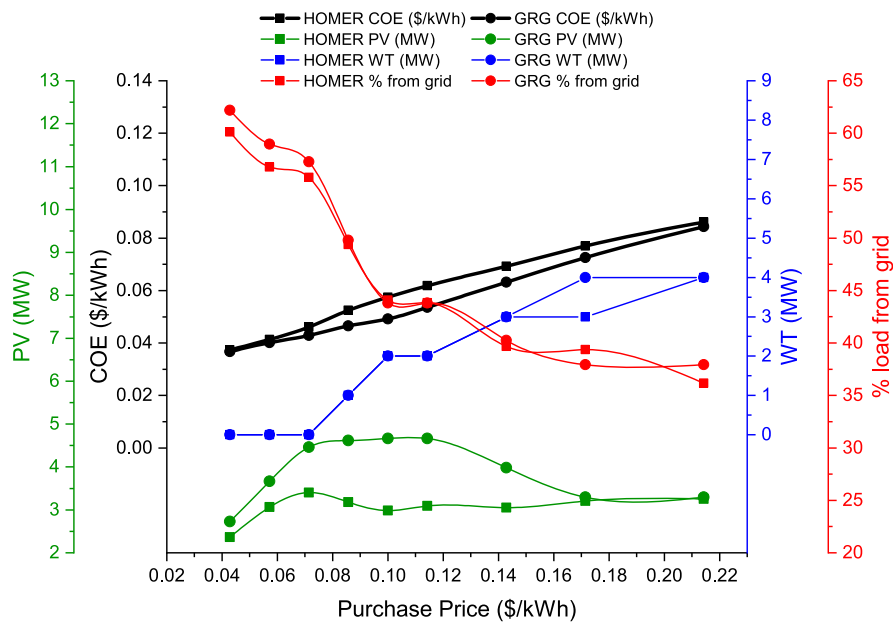


Fig. 24. Validation of GRG results for case-II of grid-connected scenario.

USD to INR conversion ratio of 1 \$ = 70 ₹ is considered in this study.

This research did not receive any specific grant from funding agencies in the public, commercial, or not-for-profit sectors.

**CRedit authorship contribution statement**

**Shebaz A. Memon:** Conceptualization, Methodology, Software, Validation, Investigation, Resources, Data curation, Writing – original draft. **Darshit S. Upadhyay:** Conceptualization, Writing – review & editing. **Rajesh N. Patel:** Conceptualization, Methodology, Writing – review & editing, Supervision.

**Declaration of Competing Interest**

None.

**References**

- [1] NREL, Costs continue to decline for residential and commercial photovoltaics in 2018, News | NREL (2018). <https://www.nrel.gov/news/program/2018/costs-continue-to-decline-for-residential-and-commercial-photovoltaics-in-2018.html> (accessed April 7, 2019).
- [2] UNFCCC, Paris Agreement, in: Conference Parties Its Twenty-First Sess, 2015. [https://unfccc.int/files/meetings/paris\\_nov\\_2015/application/pdf/paris\\_agreement\\_english.pdf](https://unfccc.int/files/meetings/paris_nov_2015/application/pdf/paris_agreement_english.pdf) (accessed September 14, 2019).
- [3] A.J. Nathan, A. Scobell, How China sees America, Foreign Aff 91 (2012) 1–38, <https://doi.org/10.1017/CBO9781107415324.004>.
- [4] A. Pérez-Navarro, D. Alfonso, H.E. Ariza, J. Cárcel, A. Correcher, G. Escrivá-Escrivá, E. Hurtado, F. Ibáñez, E. Peñalvo, R. Roig, C. Roldán, C. Sánchez, I. Segura, C. Vargas, Experimental verification of hybrid renewable systems as feasible energy sources, Renew. Energy. 86 (2016) 384–391, <https://doi.org/10.1016/j.renene.2015.08.030>.
- [5] J. Jurasz, F.A. Canales, A. Kies, M. Guezgouz, A. Beluco, A review on the complementarity of renewable energy sources: Concept, metrics, application and

- future research directions, *Sol. Energy*. 195 (2020) 703–724, <https://doi.org/10.1016/j.solener.2019.11.087>.
- [6] M.K.K. Deshmukh, S.S.S. Deshmukh, Modeling of hybrid renewable energy systems, *Renew. Sustain. Energy Rev.* 12 (2008) 235–249, <https://doi.org/10.1016/j.rser.2006.07.011>.
- [7] K. Anoune, M. Ghazi, M. Bouya, A. Lahnizi, M. Ghazouani, A. Ben Abdellah, A. Astito, Optimization and techno-economic analysis of photovoltaic-wind-battery based hybrid system, *J. Energy Storage*. 32 (2020), 101878, <https://doi.org/10.1016/j.est.2020.101878>.
- [8] W. Zhang, A. Maleki, M.A. Rosen, J. Liu, Optimization with a simulated annealing algorithm of a hybrid system for renewable energy including battery and hydrogen storage, *Energy* 163 (2018) 191–207, <https://doi.org/10.1016/j.energy.2018.08.112>.
- [9] M. Majidi, S. Nojavan, N. Nourani Esfetanaaj, A. Najafi-Ghalelou, K. Zare, A multi-objective model for optimal operation of a battery/PV/fuel cell/grid hybrid energy system using weighted sum technique and fuzzy satisfying approach considering responsible load management, *Sol. Energy*. 144 (2017) 79–89, <https://doi.org/10.1016/J.SOLENER.2017.01.009>.
- [10] A. Rathore, N.P. Patidar, Optimal sizing and allocation of renewable based distribution generation with gravity energy storage considering stochastic nature using particle swarm optimization in radial distribution network, *J. Energy Storage*. 35 (2021), 102282, <https://doi.org/10.1016/j.est.2021.102282>.
- [11] S. Sanajaoba Singh, E. Fernandez, Modeling, size optimization and sensitivity analysis of a remote hybrid renewable energy system, *Energy* 143 (2018) 719–731, <https://doi.org/10.1016/j.energy.2017.11.053>.
- [12] S. Makhdoomi, A. Askarzadeh, Optimizing operation of a photovoltaic/diesel generator hybrid energy system with pumped hydro storage by a modified crow search algorithm, *J. Energy Storage*. 27 (2020), 101040, <https://doi.org/10.1016/j.est.2019.101040>.
- [13] A. Yahiaoui, F. Fodhil, K. Benmansour, M. Tadjine, N. Cheggaga, Grey wolf optimizer for optimal design of hybrid renewable energy system PV-Diesel Generator-Battery: Application to the case of Djanet city of Algeria, *Sol. Energy*. 158 (2017) 941–951, <https://doi.org/10.1016/J.SOLENER.2017.10.040>.
- [14] A. Modarresi Ghazvini, J. Olamaei, Optimal sizing of autonomous hybrid PV system with considerations for V2G parking lot as controllable load based on a heuristic optimization algorithm, *Sol. Energy*. 184 (2019) 30–39, <https://doi.org/10.1016/J.SOLENER.2019.03.087>.
- [15] P.P. Kumar, R.P. Saini, Optimization of an off-grid integrated hybrid renewable energy system with different battery technologies for rural electrification in India, *J. Energy Storage*. 32 (2020), 101912, <https://doi.org/10.1016/j.est.2020.101912>.
- [16] C. Li, D. Zhou, H. Wang, H. Cheng, D. Li, Feasibility assessment of a hybrid PV/diesel/battery power system for a housing estate in the severe cold zone—A case study of Harbin, China, *Energy* 185 (2019) 671–681, <https://doi.org/10.1016/j.energy.2019.07.079>.
- [17] G. Zhang, B. Wu, A. Maleki, W. Zhang, Simulated annealing-chaotic search algorithm based optimization of reverse osmosis hybrid desalination system driven by wind and solar energies, *Sol. Energy*. 173 (2018) 964–975, <https://doi.org/10.1016/J.SOLENER.2018.07.094>.
- [18] A. Khiaredine, C. Ben Salah, D. Rekioua, M.F. Mimouni, Sizing methodology for hybrid photovoltaic /wind/hydrogen/battery integrated to energy management strategy for pumping system, *Energy* 153 (2018) 743–762, <https://doi.org/10.1016/j.energy.2018.04.073>.
- [19] F. Tooryan, H. HassanzadehFard, E.R. Collins, S. Jin, B. Ramezani, Optimization and energy management of distributed energy resources for a hybrid residential microgrid, *J. Energy Storage*. 30 (2020), 101556, <https://doi.org/10.1016/j.est.2020.101556>.
- [20] Z. Deng, X. Hu, X. Lin, L. Xu, Y. Che, L. Hu, General discharge voltage information enabled health evaluation for lithium-ion batteries, *IEEE/ASME Trans. Mechatronics*. (2020) 4435, <https://doi.org/10.1109/TMECH.2020.3040010>.
- [21] Z. Deng, X. Hu, X. Lin, Y. Che, L. Xu, W. Guo, Data-driven state of charge estimation for lithium-ion battery packs based on Gaussian process regression, *Energy* 205 (2020), 118000, <https://doi.org/10.1016/j.energy.2020.118000>.
- [22] X. Tang, Z. Duan, X. Hu, H. Pu, D. Cao, X. Lin, Improving ride comfort and fuel economy of connected hybrid electric vehicles based on traffic signals and real road information, *IEEE Trans. Veh. Technol.* 70 (2021) 3101–3112, <https://doi.org/10.1109/TVT.2021.3063020>.
- [23] X. Tang, T. Jia, X. Hu, Y. Huang, Z. Deng, H. Pu, Naturalistic data-driven predictive energy management for plug-in hybrid, 7 (2021) 497–508.
- [24] Y. Pu, P. Wang, Y. Wang, W. Qiao, L. Wang, Y. Zhang, Environmental effects evaluation of photovoltaic power industry in China on life cycle assessment, *J. Clean. Prod.* 278 (2021), 123993, <https://doi.org/10.1016/j.jclepro.2020.123993>.
- [25] Q. Hassan, Evaluation and optimization of off-grid and on-grid photovoltaic power system for typical household electrification, *Renew. Energy*. 164 (2021) 375–390, <https://doi.org/10.1016/j.renene.2020.09.008>.
- [26] H. Mehrjerdi, Modeling and optimization of an island water-energy nexus powered by a hybrid solar-wind renewable system, *Energy* 197 (2020), 117217, <https://doi.org/10.1016/j.energy.2020.117217>.
- [27] M. Ortega, P. del Río, P. Ruiz, W. Nijs, S. Politis, Analysing the influence of trade, technology learning and policy on the employment prospects of wind and solar energy deployment: The EU case, *Renew. Sustain. Energy Rev.* 122 (2020), 109657, <https://doi.org/10.1016/j.rser.2019.109657>.
- [28] J.H. Wong, M. Royapoor, C.W. Chan, Review of life cycle analyses and embodied energy requirements of single-crystalline and multi-crystalline silicon photovoltaic systems, *Renew. Sustain. Energy Rev.* 58 (2016) 608–618, <https://doi.org/10.1016/j.rser.2015.12.241>.
- [29] G. CEA, MoP, CDM - CO2 baseline database - central electricity authority, 2019, <https://cea.nic.in/cdm-co2-baseline-database/?lang=en> (accessed December 26, 2020).
- [30] M. Ortega-Izquierdo, P. del Río, An analysis of the socioeconomic and environmental benefits of wind energy deployment in Europe, *Renew. Energy*. 160 (2020) 1067–1080, <https://doi.org/10.1016/j.renene.2020.06.133>.
- [31] I. Renewable energy agency, renewable energy and jobs: annual review 2019, 2019, [www.irena.org](http://www.irena.org) (accessed November 7, 2020).
- [32] L.S. Lasdon, A.D. Waren, A. Jain, M. Ratner, Design and testing of a generalized reduced gradient code for nonlinear programming, *ACM Trans. Math. Softw.* 4 (2002) 34–50, <https://doi.org/10.1145/355769.355773>.
- [33] G.A. Gabriele, K.M. Ragsdell, Generalized reduced gradient method: a reliable tool for optimal design, *Am. Soc. Mech. Eng.* (1975) 394–400.
- [34] K. Rudd, G. Foderaro, P. Zhu, S. Ferrari, A generalized reduced gradient method for the optimal control of very-large-scale robotic systems, *IEEE Trans. Robot.* 33 (2017) 1226–1232, <https://doi.org/10.1109/TRO.2017.2686439>.
- [35] K. Deb, *Optimization for Engineering Design: Algorithms and Examples*, Prentice Hall of India, 1998 [https://books.google.co.in/books?id=cNkjtySMhIC&printsec=frontcover&redir\\_esc=y#v=onepage&q&f=false](https://books.google.co.in/books?id=cNkjtySMhIC&printsec=frontcover&redir_esc=y#v=onepage&q&f=false) (accessed April 10, 2019).
- [36] S.S. Rao, *Engineering Optimization: Theory and Practice: Fourth Edition*, John Wiley & Sons, Inc., Hoboken, NJ, USA, 2009, <https://doi.org/10.1002/9780470549124>.
- [37] Z. Sakhaei, R. Azin, S. Osfouri, Assessment of empirical /theoretical relative permeability correlations for gas-oil / condensate systems, *Oil. Gas Petrochem. Conf.* (2016) 1–11.
- [38] CERC-2016-17, Determination of benchmark capital cost norm for solar PV power projects and solar thermal power projects applicable during FY 2016-17, *Cent. Electr. Regul. Comm.* (2016) 1–31. <http://www.cercind.gov.in/2016/orders/SO17.pdf>.
- [39] Gujarat Electricity Regulatory Commission (GERC), Gujarat electricity regulatory commission (GERC) - Order No. 2 of 2016 - determination of tariff for wind power projects, *Gujarat Electr. Regul. Comm.* (2016) 1–41. <http://gercin.org/uploaded/document/07c74229-5dc4-4406-89d3-25a82fa0931b.pdf>.
- [40] Ministry of New and Renewable Energy (MNRE), *Economic rate of return of various renewable energy technologies*. Ministry of New and Renewable Energy (MNRE), Government of India, 2018 <http://www.indiaenvironmentportal.org.in/files/file/Draft-Report-Study-on-ERR-for-RETS.pdf>.
- [41] A. Abdelkader, A. Rabeh, D. Mohamed Ali, J. Mohamed, Multi-objective genetic algorithm based sizing optimization of a standalone wind/PV power supply system with enhanced battery/supercapacitor hybrid energy storage, *Energy* 163 (2018) 351–363, <https://doi.org/10.1016/j.energy.2018.08.135>.
- [42] E. Ofry, A. Braunstein, The loss of power supply probability as a technique for designing stand-alone solar electrical (photovoltaic) systems, *IEEE Trans. Power Appar. Syst.* (1983) 1171–1175, <https://doi.org/10.1109/TPAS.1983.318057>.
- [43] H. Hondo, Y. Moriizumi, Employment creation potential of renewable power generation technologies: A life cycle approach, *Renew. Sustain. Energy Rev.* 79 (2017) 128–136, <https://doi.org/10.1016/j.rser.2017.05.039>.
- [44] R.H. Crawford, Life cycle energy and greenhouse emissions analysis of wind turbines and the effect of size on energy yield, *Renew. Sustain. Energy Rev.* 13 (2009) 2653–2660, <https://doi.org/10.1016/j.rser.2009.07.008>.
- [45] S. Wang, S. Wang, J. Liu, Life-cycle green-house gas emissions of onshore and offshore wind turbines, *J. Clean. Prod.* 210 (2019) 804–810, <https://doi.org/10.1016/j.jclepro.2018.11.031>.
- [46] B. Guezuraga, R. Zauner, W. Pölz, Life cycle assessment of two different 2 MW class wind turbines, *Renew. Energy*. 37 (2012) 37–44, <https://doi.org/10.1016/j.renene.2011.05.008>.
- [47] D.C. Handbook, *District Census handbook*, in: *Census India 2011 GUJARAT Ser. PART-XII-A*, 2011.
- [48] NREL, *NSRDB data viewer*, Natl. Renew. Energy Lab. (2015). <https://maps.nrel.gov/nsrdb-viewer/> (accessed January 22, 2018).
- [49] M. Sengupta, Y. Xie, A. Lopez, A. Habte, G. Maclaurin, J. Shelby, The national solar radiation data base (NSRDB), *Renew. Sustain. Energy Rev.* 89 (2018) 51–60, <https://doi.org/10.1016/J.RSER.2018.03.003>.
- [50] Gujarat Energy Transmission Corporation Limited (GETCO), *State Load Dispatch Centre (SLDC) Annual report 2017-18*, Vadodra 390021, Gujarat, INDIA, 2018 [https://doi.org/https://www.sldcguj.com/comppdoc/SLDC Annual Report 2017-18.pdf](https://doi.org/https://www.sldcguj.com/comppdoc/SLDC%20Annual%20Report%2017-18.pdf).
- [51] S.A. Hsu, E.A. Meindl, D.B. Gilhousen, S.A. Hsu, E.A. Meindl, D.B. Gilhousen, Determining the Power-Law Wind-Profile Exponent under Near-Neutral Stability Conditions at Sea, *J. Appl. Meteorol.* 33 (1994) 757–765, [https://doi.org/10.1175/1520-0450\(1994\)033<0757:DTPLWP>2.0.CO;2](https://doi.org/10.1175/1520-0450(1994)033<0757:DTPLWP>2.0.CO;2).
- [52] GERC, GERC Order No. 3 of 2015: Determination of tariff for procurement of power by distribution licensees and others from solar energy projects for the state of Gujarat., 2015.
- [53] GERC, Determination of tariff for procurement of power by the distribution licensees and others from wind power projects, 2016.
- [54] GERC, GERC Order No. 1 of 2018: Determination of tariff for procurement of power by the distribution licensees and others from biomass based power projects and bagasse based co-generation projects for the state of Gujarat, 2018.
- [55] S. Agarwal, N. Bali, J. Urpelainen, Rural electrification in India: customer behaviour and demand, 2019.
- [56] B.E. Türkay, A.Y. Telli, Economic analysis of standalone and grid connected hybrid energy systems, *Renew. Energy*. 36 (2011) 1931–1943, <https://doi.org/10.1016/j.renene.2010.12.007>.

- [57] M. Usman, M.T. Khan, A.S. Rana, S. Ali, Techno-economic analysis of hybrid solar-diesel-grid connected power generation system, *J. Electr. Syst. Inf. Technol.* 5 (2018) 653–662, <https://doi.org/10.1016/j.jesit.2017.06.002>.
- [58] N. & R.E. Ministry, NATIONAL WIND-SOLAR HYBRID POLICY, 2018.
- [59] Government of Gujarat Energy and Petrochemicals Department, Gujarat Wind-Solar Hybrid Power Policy-2018, Gandhinagar, 2018. [https://guj-epd.gujarat.gov.in/uploads/Gujarat\\_Wind-Solar\\_Hybrid\\_Power\\_Policy-2018.pdf](https://guj-epd.gujarat.gov.in/uploads/Gujarat_Wind-Solar_Hybrid_Power_Policy-2018.pdf).
- [60] P. Choudhary, R.K. Srivastava, Sustainability perspectives- a review for solar photovoltaic trends and growth opportunities, *J. Clean. Prod.* 227 (2019) 589–612, <https://doi.org/10.1016/J.JCLEPRO.2019.04.107>.
- [61] P. Enevoldsen, G. Xydis, Examining the trends of 35 years growth of key wind turbine components, *Energy Sustain. Dev.* 50 (2019) 18–26, <https://doi.org/10.1016/J.ESD.2019.02.003>.
- [62] Battery Power's Latest Plunge in Costs Threatens Coal, Gas | BloombergNEF, 2019 (n.d.), <https://about.bnef.com/blog/battery-powers-latest-plunge-costs-threatens-coal-gas/> (accessed, September 15).
- [63] M. Del Negro, D. Giannone, M.P. Giannoni, A. Tambalotti, Global trends in interest rates, *J. Int. Econ.* 118 (2019) 248–262, <https://doi.org/10.1016/J.JINTECO.2019.01.010>.
- [64] M.A. Aktar, M.M. Alam, A.Q. Al-Amin, Global economic crisis, energy use, CO<sub>2</sub> emissions, and policy roadmap amid COVID-19, *Sustain. Prod. Consum.* 26 (2020) 770–781, <https://doi.org/10.1016/j.spc.2020.12.029>.
- [65] X. Shen, C. Cai, H. Li, Socioeconomic restrictions slowdown COVID-19 far more effectively than favorable weather-evidence from the satellite, *Sci. Total Environ.* 748 (2020), 141401, <https://doi.org/10.1016/j.scitotenv.2020.141401>.
- [66] A European Green Deal, European Commission, (n.d.), 2021. [https://ec.europa.eu/info/strategy/priorities-2019-2024/european-green-deal\\_en](https://ec.europa.eu/info/strategy/priorities-2019-2024/european-green-deal_en). accessed January 16.
- [67] HOMER Energy, HOMER Pro, Microgrid Software for Designing Optimized Hybrid Microgrids, 2018. <https://www.homerenergy.com/products/pro/index.html> (accessed August 16, 2019).
- [68] P. Lilienthal, P. Gilman, HOMER modelling software, *Natl. Renew. Energy Lab* (2004). <http://www.nrel.gov/homer>.
- [69] S. Bahramara, M.P. Moghaddam, M.R. Haghifam, Optimal planning of hybrid renewable energy systems using HOMER: A review, *Renew. Sustain. Energy Rev.* 62 (2016) 609–620, <https://doi.org/10.1016/j.rser.2016.05.039>.
- [70] B.K. Das, M. Hasan, Optimal sizing of a standalone hybrid system for electric and thermal loads using excess energy and waste heat, *Energy* 214 (2021), 119036, <https://doi.org/10.1016/j.energy.2020.119036>.
- [71] M.J. Khan, A.K. Yadav, L. Mathew, Techno economic feasibility analysis of different combinations of PV-Wind-Diesel-Battery hybrid system for telecommunication applications in different cities of Punjab, India, *Renew. Sustain. Energy Rev.* 76 (2017) 577–607, <https://doi.org/10.1016/j.rser.2017.03.076>.
- [72] H. Zahboune, S. Zouggar, G. Krajacic, P.S. Varbanov, M. Elhafyani, E. Ziani, Optimal hybrid renewable energy design in autonomous system using modified electric system cascade analysis and homer software, *Energy Convers. Manag.* 126 (2016) 909–922, <https://doi.org/10.1016/j.enconman.2016.08.061>.
- [73] F.H. Jufri, D.R. Aryani, I. Garniwa, B. Sudiarto, Optimal battery energy storage dispatch strategy for small scale isolated hybrid renewable energy system with different load profile patterns, *Energies* (2021) 14, <https://doi.org/10.3390/en14113139>.
- [74] H. Zahboune, S. Zouggar, G. Krajacic, P.S. Varbanov, M. Elhafyani, E. Ziani, Optimal hybrid renewable energy design in autonomous system using modified electric system cascade analysis and homer software, *Energy Convers. Manag.* 126 (2016) 909–922, <https://doi.org/10.1016/J.ENCONMAN.2016.08.061>.
- [75] A. Al-Sharafi, A.Z. Sahin, T. Ayar, B.S. Yilbas, Techno-economic analysis and optimization of solar and wind energy systems for power generation and hydrogen production in Saudi Arabia, *Renew. Sustain. Energy Rev.* 69 (2017) 33–49, <https://doi.org/10.1016/j.rser.2016.11.157>.
- [76] M.H. Amrollahi, S. Mohammad, T. Bathaee, S.M.T. Bathaee, Techno-economic optimization of hybrid photovoltaic/wind generation together with energy storage system in a standalone micro-grid subjected to demand response, *Appl. Energy*. 202 (2017) 66–77, <https://doi.org/10.1016/j.apenergy.2017.05.116>.